Aalto University
School of Chemical
Engineering

Anik Nath

ASSESSING THE ENERGY CONSUMPTION OF THE CHEMICAL RECOVERY OF GVL FROM THE BIOMASS FRACTIONATION SPENT LIQUOR

Master´s Programme in Chemical, Biochemical and Materials Engineering

Major in Chemical Engineering

Master's thesis for the degree of Master of Science in Technology submitted for inspection, Espoo, 08 October 2019.

Supervisor Professor Herbert Sixta

Instructor DSc. Juha-Pekka Pokki

Author Anik Nath

Title of thesis Assessing the energy consumption of the chemical recovery of GVL from the biomass fractionation spent liquor

Degree Programme Chemical, Biochemical and Materials Engineering

Major Chemical Engineering

Thesis supervisor Professor Herbert Sixta

Thesis advisor(s) / Thesis examiner(s) Juha-Pekka Pokki

Date 08.10.2019 **Number of pages** 72+8 **Language** English

Abstract

This study was aimed to assess the energy consumption for GVL solvent recovery from spent liquor from a biomass fractionation process. To carry out the thermodynamic simulation study of main components such as GVL, furfural, CO_2 and water has been selected. Selection of thermodynamic models was decided based on the model decision tree and literature sources. The process was divided into three steps where liquid-liquid extraction was carried out to separate water from the GVL, compression of CO_2 was carried out for recycling and finally, vacuum distillation of GVL and furfural was carried out.

In the beginning, sensitivity analysis for vacuum distillation was conducted where different operating parameters such as no. of theoretical stages, feed composition, reflux ratio effect on GVL and furfural separation was studied using UNIF-DMD method. It was found that feed composition and reflux ratio play a significant role in separation efficiency. In addition, increasing reflux ratio is energy intensive. Another simulation case study conducted adding stripping columns prior to the distillation column allows the majority of GVL removal. Therefore, it enables less energy requirement to distillate the GVL and furfural with better separation yield.

During CO_2 compression simulation, it was assumed no impurities such as water and GVL entered the compressor. Threes stage compression simulation using REFPROP (Reference fluid properties equation state developed by NIST) was carried out to pressurize CO_2 at 7.5 MPa and at outlet temperature of 298K which therefore recycles back to the liquid-liquid extraction column.

Finally, liquid-liquid extraction was simulated based on the correlated measured distribution coefficients published prior to this work. In the process, it was studied enabling three stages of the decanting. Each separation stages uses a correlation based on the measured LLE. The out-stream of extracting columns showed a satisfactory result of removing the water phase. The overall GVL recovery process of energy consumption calculated based on the GVL feed mass flow rate and the calculated energy consumption is 6088.52 $kJkg^{-1}$ GVL in the feed. The calculated results show that the compressor is the highly energy-intensive unit in the process which consumes approximately ≈92% of the total energy and requires 5657.15 $kJkg^{-1}$ GVL in feed.

Keywords Biomass, γ-valerolactone, GVL, Furfural, Thermodynamic model, Solvent Recovery

Contents

Preface

At first, I would like to take this opportunity to thank Professor Herbert Sixta for giving me the opportunity to work in his research team and for his continuous support. Also, I like to thank my instructor DSc. Juha-Pekka Pokki for his all technical supports and instructions throughout the thesis period and during report writing. In addition, thanks to Huy Quang Lê for sharing his ideas at a different stage of the thesis.

I would like to thank all my friends, family members and especially my mother Chinmoyee Prava Devi for always being supportive and for her inspirations, which still keeps me moving forward.

Dedication

I dedicate this thesis work to my father Late. Haradhan Nath whom life ethics always been my motivation.

1. Introduction

During the late 20th century, at least four industry trends played a role behind for implementing the term bio-refinery. Followed by the literature, the first industrial trend was, increased awareness regarding the utilization of biomass resources in more economically and environmentally friendly. Secondly, the growing interest in upgrading more low-quality lingo-cellulosic biomass into more valuable product played a key role. As third, the attention came into the production of starch for energy applications. Finally, the realization of developing high-value products and diversify the product mix in order to meet global competition by utilising the excess amount of biomass in many industries found the importance of bio-refinery (Thore, Sandén et al. 2012). The definition of bio-refinery was given in several ways in many studies. One of the most widely used definition was given by the member of IEA Bioenergy task 42 is "Bio-refinery is the sustainable processing of biomass into a spectrum of marketable products (food, feed, materials, and chemicals) and energy (fuels, power, heat)" (Sonnenberg, Baars et al. 2007) .

Our study scope based on a novel biorefinery concept developed in the department of bioproducts and bio-systems at Aalto University as part of a doctoral study carried out by Huy Quang Lê under the supervision of Professor. Herbert Sixta. A developed novel bio-refinery concept introduced a shortcut process for converting wood biomass to textile fibres using the mixture of γ-valerolactone (GVL) and water. The general block diagram of the novel bio-refinery process concept extracted from the available literature given below as in *Figure 1*

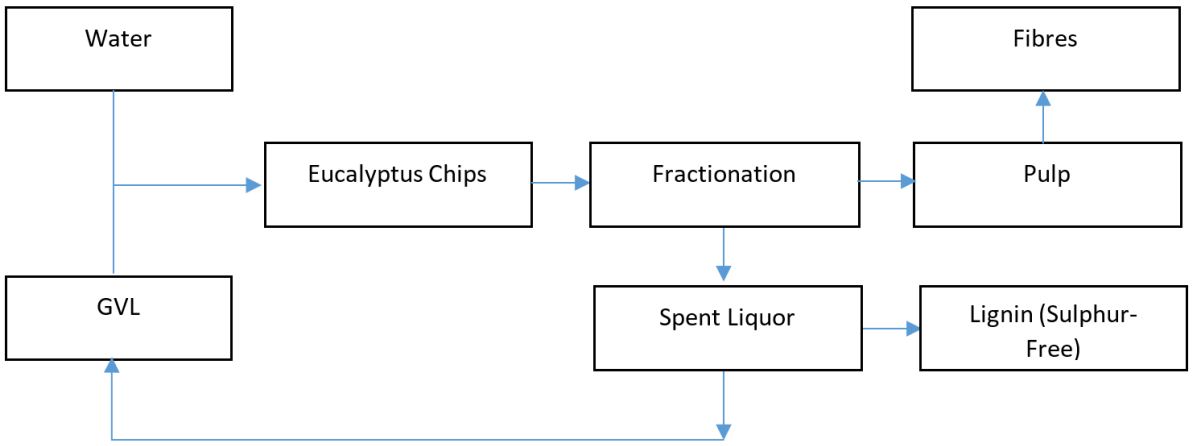

Figure 1. Conceptual block diagram of converting wood biomass to textile fibres using GVL solvent (Le, Huy, Pokki et al. 2017)

GVL is known as one of the versatile chemical compound used in various industries such as (food industries, pulp and paper industries etc.). It is a naturally occurred chemical, which can be originated from lignocellulosic biomass resources. Therefore, it can be considered as a green solvent with very promising characteristics compared to other commercially and industrially used solvents. Different characteristics such as renewability, no-toxicity and biodegradability made it more appealing to industrial uses in consideration of environmental safety (Tang, Zeng et al. 2014). The physicochemical properties of the pure GVL described in later section 4 below of literature part.

According, to *Figure 1* novel bio-refinery concept, an optimum mixture of GVL and water used to carry out the fractionation of eucalyptus wood biomass. The use of a binary mixture of GVL and water as solvent and reaction medium for the fractionation was suggested in a study conducted by (Fang, Sixta 2015). Followed by the study, the process led it to the recovery of pure cellulose, uniform sugar components from hemicellulose and a pure lignin fraction. Findings show that using GVL and water binary mixture as a solvent the yield of the pulp residue could reach 40.3 % with a high cellulose purity of 90.3 % (Fang, Sixta 2015).

However, the recovery of GVL solvent and recycling makes the process itself cheaper and sustainable by reducing the use of extra pure GVL. As the process involves a binary mixture of GVL and water, it requires further purification process before recycling back to the main process. According to a study conducted by (Le, Huy Quang, Ma et al. 2016) shows that formulated spent liquor from the fractionation process contains extracted carbohydrates and their degradation products. Followed by the analysis results, degradation reaction produces furans (furfural, hydroxymethylfurfural) and organic acids such as (formic acid, acetic acid and levulinic acid) etc. (Le, Ma et al. 2016). Therefore, the recovery of pure GVL becomes more complex as it contains a mixture of many chemical substances.

2. Aim of the study

It was assumed to be that economic feasibility and sustainability of novel bio-refinery process could be improved by recycling GVL, which led it to this master's thesis for assessing energy consumption for the GVL recovery process. Therefore, the main objective of the thesis decided to assess the energy consumption during the GVL recovery process. Previously mentioned that the spent liquor after fractionation process contains different types of degradation products, organic acids and hydrocarbons. Consequently, the purification process must be employed to achieve pure GVL prior to the recycle to the system. Here the overall biomass fractionation process and solvent recovery block diagram are given below. The study scope for assessing the energy consumption of GVL recovery well-defined by the red area is given as in *Figure 2*.

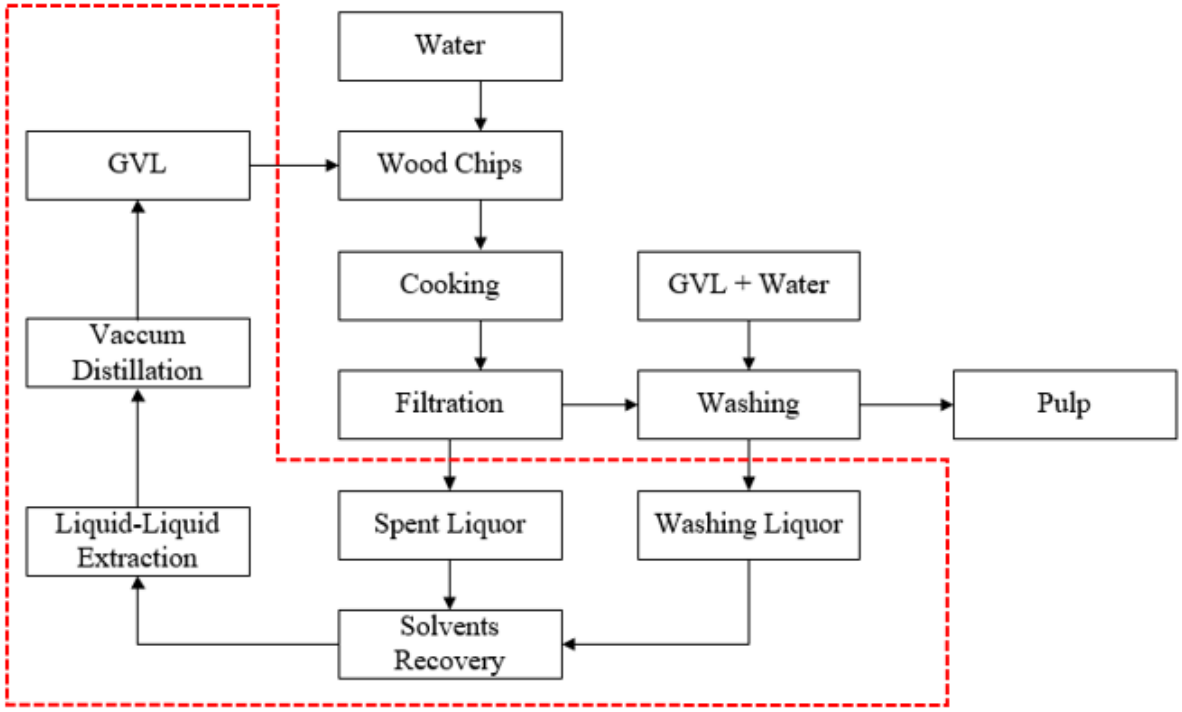

Figure 2. Block diagram of the GVL recovery from washing liquid and spent liquor (red rectangular box defines thesis study scope)

A diagram of the possible route of GVL separation process, which involves a few stages provides an insight look of the process given as Figure 3.

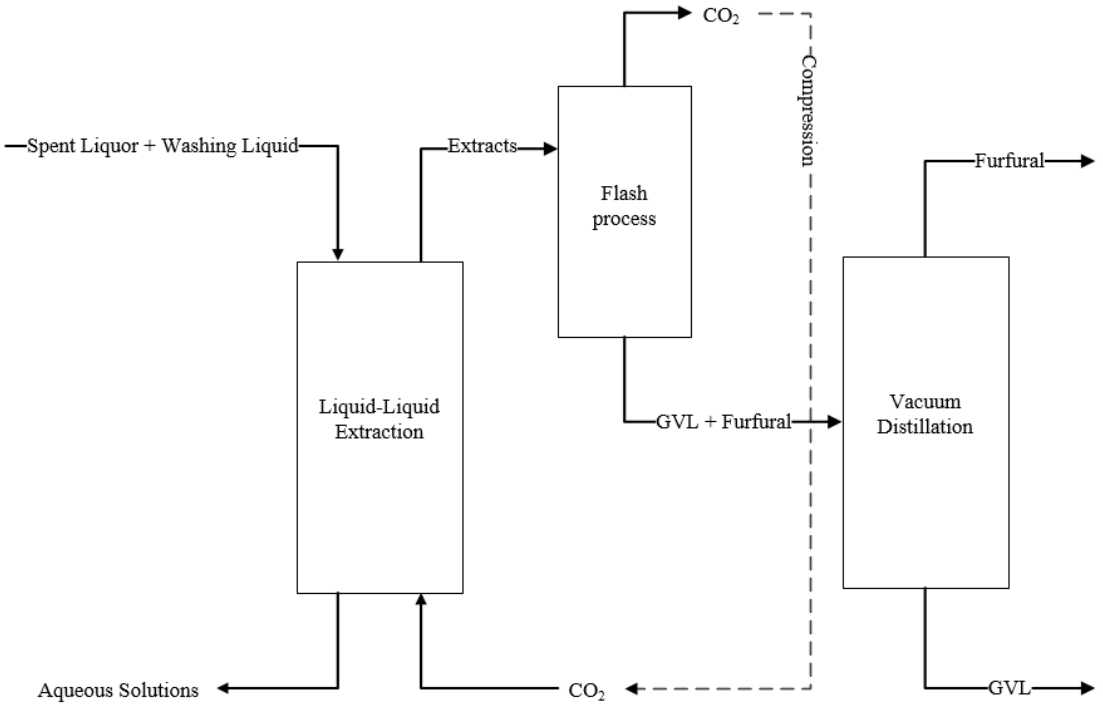

Figure 3. Conceptual detailed diagram of different separation stages for GVL recovery from biomass fractionation spent liquor.

Followed by Figure 3, it was modelled that, separation stages will take places in different stages such as liquid-liquid extraction using CO_2 in its near supercritical state, separation of CO_2 followed by the flash process when its depressurized and vacuum distillation of furfural and GVL.

To continue further work on separation stages, thermodynamic properties for the main elements will be required to be collected. In this study, the thermodynamic simulation will be carried out for an understanding of system behaviour in different components of mixtures conditions. This developed novel bio-refinery process utilized hardwood biomass fractionation by using GVL and water. Therefore, GVL, furfural, water and CO_2 were considered as the main elements to study. However, implementing the process in large scale requires a detailed understanding of energy consumption for the chemical recovery of GVL using liquid CO_2 near its critical condition. Therefore, we will mainly focus on the energy consumption in terms of the maximum percentage of chemical recovery of GVL solvent from spent liquor after filtration and washing (red area) *Figure 2*.

In this thesis study, we demonstrated the simulation of individual models of liquid-liquid extraction using CO_2 near its critical condition, flash process separation of CO_2 and vacuum

distillation process for GVL and furfural recovery using Aspen Plus simulation software. As part of this demonstration, thermodynamic models have been applied. Also, sensitivity analysis by operating parameters changes such as reflux ratio, number of stages in the column, number of columns and so on will be studied to describe possible GVL and furfural separation.

Literature Review

3. Biomass & derivatives

In this part of the literature, a general discussion about different biomass and available bio-refineries in operation is presented. By the description, biomass is organic matters like wood, crops, seaweed and animal wastes, which can be utilized to convert it to the useable energy. The process starts from the photosynthesis where sunlight energy used to convert water and carbon dioxide into oxygen and sugars. These sugars also called as carbohydrates deliver the energy to an animal whose eat plants. In sum, it can be described that, a form of energy changes from radiant to chemical energy. Biomass also knowns as the oldest energy source after the sun. Also, biomass like plants and trees, which is abundant naturally on the earth. Moreover, the biomass sources like trees, corns and other plants can be planted. Nowadays there are four types of biomass get used in, which are wood and agricultural products, solid waste, landfill gas & biogas, alcohol fuels (The NEED project 2017). A lignocellulosic process flow below shows the biomass to different products like energy and biomaterials as in Figure 4 (Stöcker 2008).

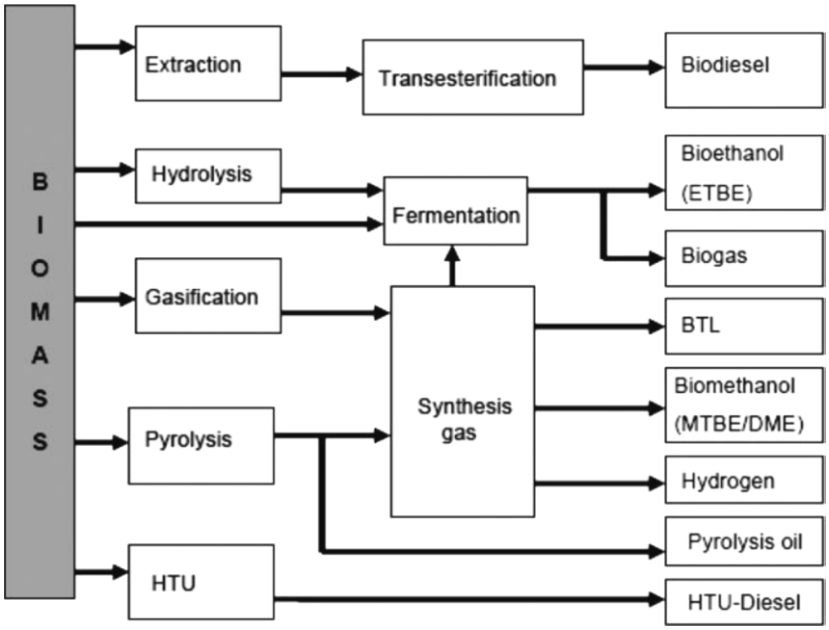

Figure 4: Simplified lignocellulosic bio-refinery process flow diagram (Stöcker 2008).

Followed by the figure above, it can be seen that, there are many routes or production methods can be followed to produce selective materials as end products. Apart from the biomass to energy or fuel conversion, woody biomass is widely used in the pulp and paper industry as well. The wood biomass compositions typically consist of 70% cellulosic carbohydrates (≈ 40

% dry weight of cellulose and 25% of the dry weight of hemicellulose) and 25% of the dry weight of lignin (Sjostrom 2013). Even though pulp predominantly used for paper production, the use of pulp from woody biomass is also to derive different cellulose derivatives such as rayon silk and cellophane (Sjostrom 2013).

4. Physical & chemical properties of components

In this section of the literature studies, it will be discussed physicochemical properties of different main components selected for our study. Therefore, the selection of chemical components based on predominance among many others in the selected part of the GVL recovery process. Selection of main components also helps to avoid complicacy during thermodynamic modelling in its preliminary stage. The idea was to understand systems like binary or, ternary during the separation process and so on. Thereafter, knowledge and findings from systems like a binary mixture of compounds can be transferred to design multi-component system, which will represent the industrial process more realistic way.

Followed by the chemical analysis conducted by the (Le, Ma et al. 2016) in the novel biorefinery concept shows that, the process spent liquor consists of components like cellulose, hemicellulose, lignin, furfural, HMF and organic acids. According to the description, the organics acids are more specifically formic acid, acetic acid and levulinic acid. Composition of the different components given as table below which was extracted from the (Le, Ma et al. 2016) study on spent liquor analysis. However, the spent liquor considered to be as the sum of free spent liquor and washing liquids. Fractionation and washing process conducted using GVL and water, which results in the presence of GVL and water is obvious in spent liquor.

Table 1: Components composition in spent liquor extracted after fractionation of eucalyptus chips in GVL/Water (Le, Ma et al. 2016).

		Wood components (% odw)					
		Spent liquor[c]					
GVL[a]	Time[b]	Cellulose	Hemicellulose	Lignin[d]	Furfural	HMF	Acids[e]
50	60	0.8	9.2	26.8	1.5	0.1	8.5
50	90	0.4	7.8	26.9	2.5	0.2	9.5
50	120	0.5	6.5	27.8	3.7	0.3	8.5
50	150	0.5	5.1	28	4.8	0.4	8.1
50	180	0.6	4.1	28.1	5.6	0.5	7.8
60	60	0.4	8.1	24.7	1	0.1	8.4
60	90	0.4	7.7	26.3	1.9	0.1	10.1
60	120	0.3	5.7	28.2	3	0.2	10.3
60	150	0.4	4.9	27.6	3.2	0.3	9
60	180	0.5	4.3	28.1	4.5	0.4	9.9

[a] GVL content in fractionation liquor (in wt%). [b] Fractionation time (in minutes). [c] Spent liquor is considered to be as the sum of free spent liquor and washing liquids. [d] Unextracted wood shown as lignin amount. [e] Organic acids: formic acid, acetic acid and levulinic acid.

The analysis results above *Table 1* shows that, the extracted components composition changes with different operating parameters like GVL content in fractionation liquor and fractionation time. The optimum parameters were found with 50 wt% and 60 minutes fractionation time, in which achieved high pulp (cellulose, hemicellulose, lignin) yield % of (45.8 %, 4.4%, 2,6%) respectively, which can be flowed in (Le, Ma et al. 2016). However, in spent liquor, it can be seen some amount of pulp contents still exists. Therefore, filtration, vacuum distillation and superfluid liquid extraction using CO_2 were employed in laboratory scale to separate lignin, remove water and extract furfural, HMF and organic acids. A schematic flow diagram of the separation process given below as in *Figure 5*.

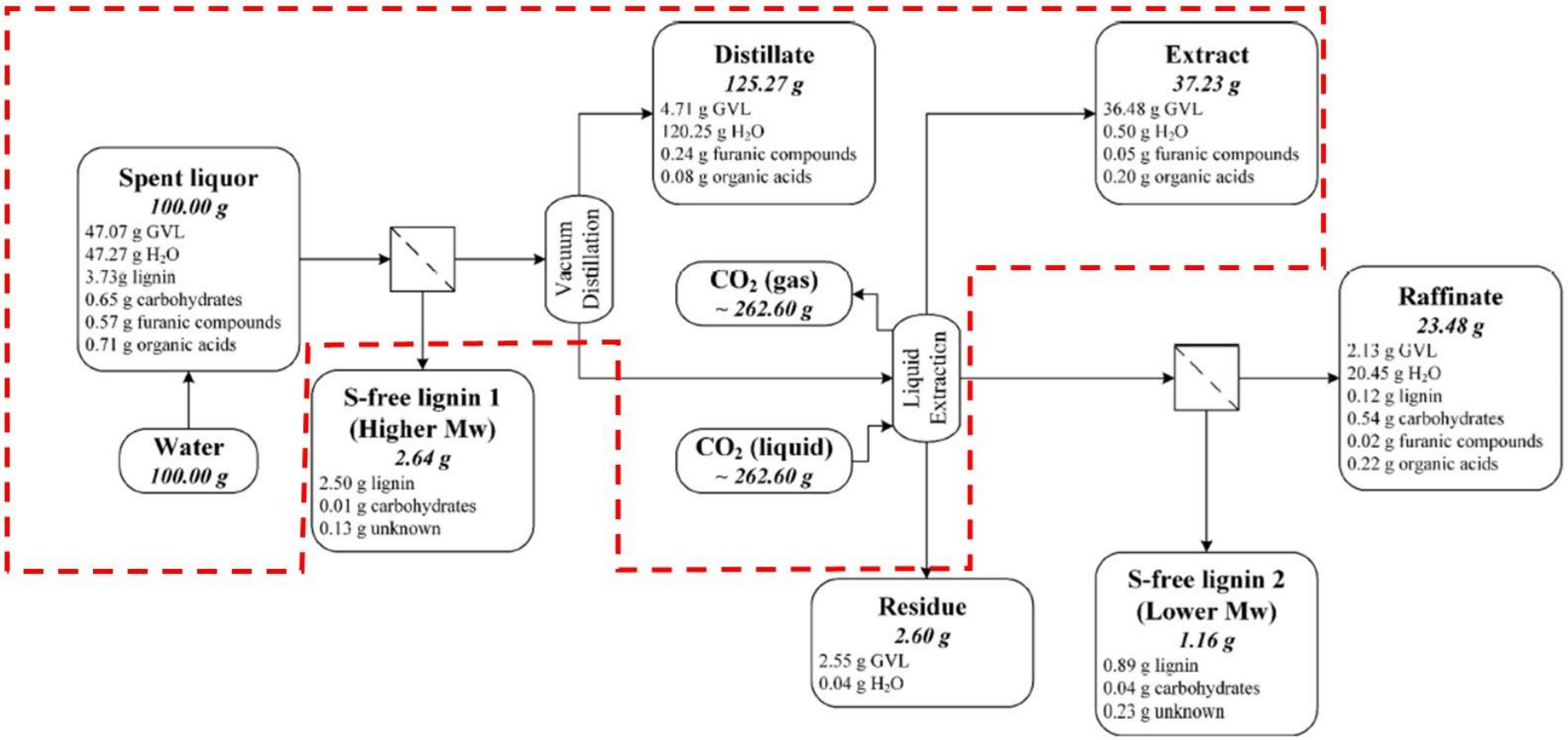

Figure 5. A separation process flow diagram of Lignin, GVL, Water and other contents from spent liquor in laboratory scale (Lê, Pokki et al. 2018)

The mass balance in the process flow diagram based on a recovery scheme carried out in laboratory-scale conducted by (Lê, Pokki et al. 2018). In our study, we focused on, spent liquor, extract and distillate values given in *Figure 5*. As we mentioned earlier, to simplify the thermodynamic study and simulation, we will be focused only on main components like GVL, water, furfural and CO_2. Therefore, the pure components physicochemical properties data of main components presented as in *Table 2*.

Table 2: The physicochemical properties of the main components of study interest

	Components			
	Carbon dioxide	**Water**	**GVL**	**Furfural**
Molecular formula	**CO_2**	**H_2O**	**$C_5H_8O_2$**	**$C_5H_4O_2$**
CAS No.	124-38-9	7732-18-5	108-29-2	98-01-1
Molecular weight, g/mol	44.01	18.02	100.12	96.08
Boiling point, K	194.67	373.12	480.65	434.85
Critical temperature, T_c, K	304.19	647.10	727.00	670.15
Critical pressure, P_c, bar	73.82	220.64	48.4	56.6
Critical density , ρ_c, (g/mL)	0.468	0.322	-	0.381
Critical compressibility factor, Z_c	0.274	0.229	0.223	0.256
Acentric factor, ω	0.228	0.345	0.403	0.368

4.1 GVL and GVL based Solvents

According to (Fegyverneki, Orha et al. 2010), in terms of gaining the sustainability in the chemical industry and ensure the safe use of chemicals in various applications purpose, it was required to develop solvents which can address physical and chemical challenges. In addition to these definite requirements of the physical and chemical properties to perform solvent functions, it is also preferable to derive more new green solvents, which are also featured with biodegradability, no or low toxicity, renewable by following the fifth principle of green chemistry (Anastas, Warner 2000) (Kerton, Marriott 2013). As it was mentioned earlier, due to the excellent physical and chemical properties of GVL, it is considered as a great solvent. Other GVL based solvents such as methyl 4-methoxyvalerate, ethyl 4-ethoxyvalerate were synthesized and characterized by (Fegyverneki, Orha et al. 2010). A temperature-dependent vapour pressure comparison between the synthesized solvents, GVL and other oxygenates presented in their study. The observation of vapour pressure changes with temperature changes has been plotted, which is presented below as *Figure 6* (Fegyverneki, Orha et al. 2010).

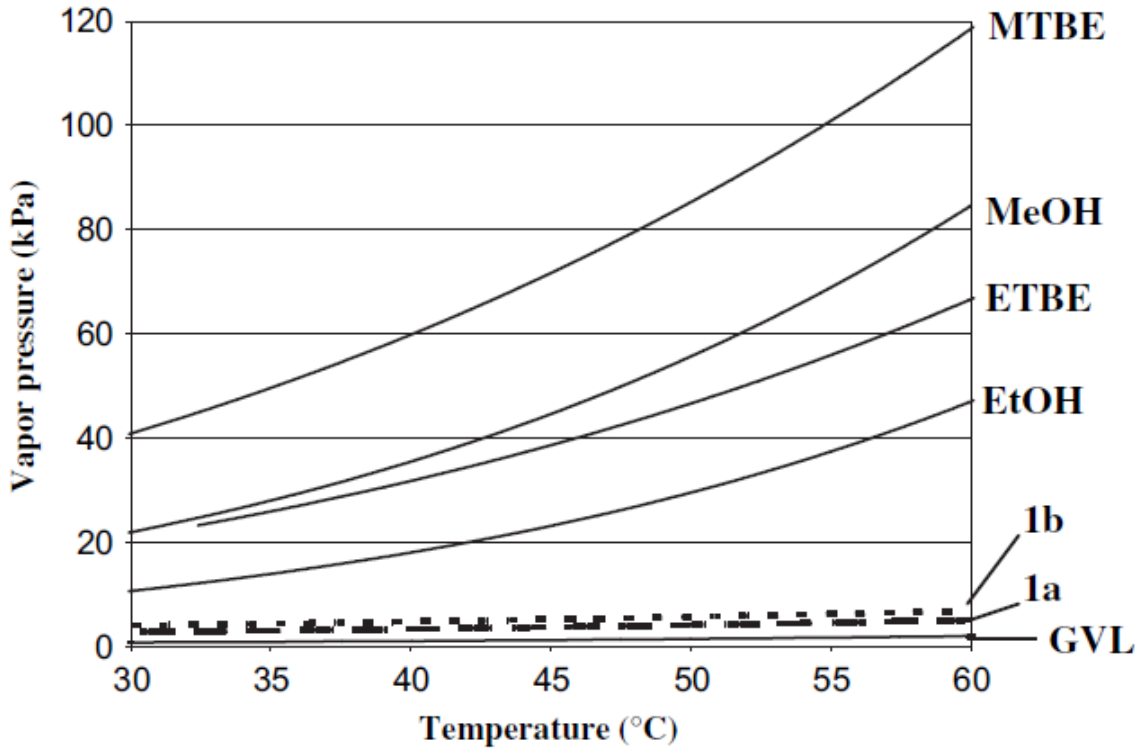

1a = methyl 4-methoxyvalerate
1b = ethyl 4-ethoxyvalerate

Figure 6: Vapour pressure plot with temperature changes for GVL, GVL based derivatives and other oxygenates (Fegyverneki, Orha et al. 2010)

According to *Figure 6*, it is noticeable that temperature increment from 30-60℃, does not exhibit significant increase f vapour pressure for GVL. In addition, GVL based derivatives also show almost no increasing trends of vapour pressure increment with temperature increase. However, GVL derivatives exhibit a negligibly higher amount of vapour pressure than pure GVL, while other oxygenates like MTBE, MeOH, EtOH and ETBE shows quite a large amount of vapour pressure effects ranges between 20 -120 KPa. Therefore, in terms of vapour pressure properties, GVL and GVL based solvents like methyl 4-methoxyvalerate, ethyl 4-ethoxyvalerate makes it more appealing and makes the opportunity to choose alternatives.

As in our system contains GVL, we must consider our GVL properties and their effects. There were few studies have been conducted to define the vapour pressure effect of GVL with higher temperature. In (Havasi, Mizsey et al. 2016) study, it was presented the vapour pressure of GVL and compared their measure and calculated values with other studies. Here, temperature-dependent vapour pressure plot in 238 – 455 K given as in *Figure 7*.

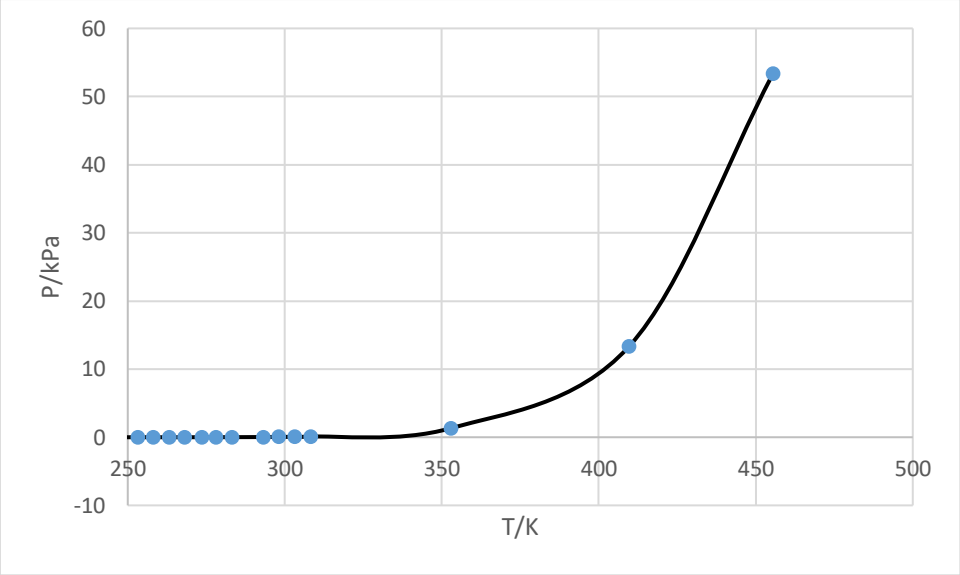

Figure 7: Vapour pressure, Liquid and Temperature plot for GVL. (Leonard 1956, Pokorný, Štejfa et al. 2017)

a = temperature range 350-460 K, b = temperature range 250-320 K

From above *Figure 7*, it can be seen that the vapour pressure rises significantly for GVL above 70℃ ($\approx 340\ K$). According to(Havasi, Mizsey et al. 2016), it requires GVL vapour pressure to reach equal to the atmospheric pressure 101.325 kPa very high temperature approximately to 478.0K. However, specific vapour pressure data points as a function of temperature can be extracted from different literature sources.

Here, the individual temperature-independent properties of GVL can be found in *Table 22* below in Appendix 1.

4.2 Carbon Dioxide

In this thesis study, the use of compressed carbon dioxide was as the liquid solvent below its supercritical temperature (≈ 25℃) to conduct the liquid-liquid extraction. However, The uses of supercritical carbon dioxide as the solvent is well established in many applications such as polymer modification, the formation of polymer composites, microcellular foaming, particle production and so on (Nalawade, Picchioni et al. 2006). The reason carbon dioxide position itself ahead than any other solvents because of reaching its critical state comparably in lower temperature. Followed by (McHugh, Krukonis 2013) in their book, it was compared the critical temperature and critical pressure of many solvents. Some of them are tabulated here as in *Table 3* for comparison (McHugh, Krukonis 2013).

Table 3: Critical conditions for various solvents(McHugh, Krukonis 2013)

Solvents	Critical Temperature, K	Critical Pressure, MPa
Carbon dioxide	304.3	7.4
Ethane	305.4	4.9
Propane	369.9	4.3
Propylene	365.1	4.6
Cyclohexane	553.5	4.0
Benzene	562.2	4.9
Toluene	591.8	4.1
p-Xylene	616.3	3.5
Ammonia	405.7	11.3
Water	647.4	22.1

A phase diagram for carbon dioxide defines the state different phases with the change of temperature and pressure. In a book chapter of (Witkowski 2015), illustrated the phase diagram of carbon dioxide, which is present below as Figure 8.

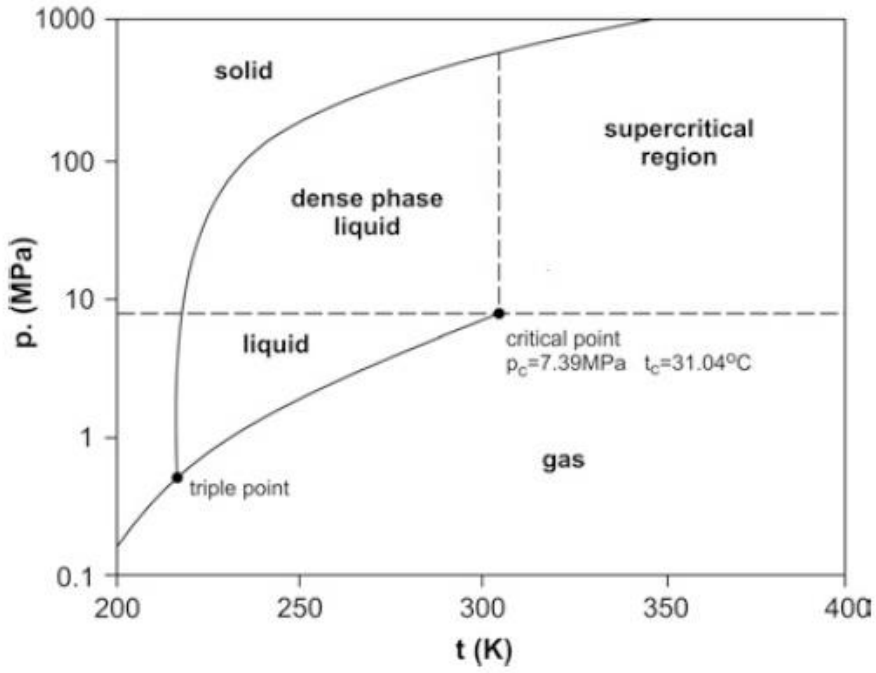

Figure 8: A phase diagram of carbon dioxide (Witkowski 2015)

From *Figure 8*, it can be seen that to maintain the supercritical state of the carbon dioxide, it is required to have the system temperature above 31.04 ℃ and the pressure above 7.39 MPa. However, our system operating temperature is below its supercritical region. The basic physicochemical properties of the carbon dioxide already presented in *Table 2* above. Vapour

pressure experimental extracted data blow its supercritical region for CO_2 given below as *Figure 9*.

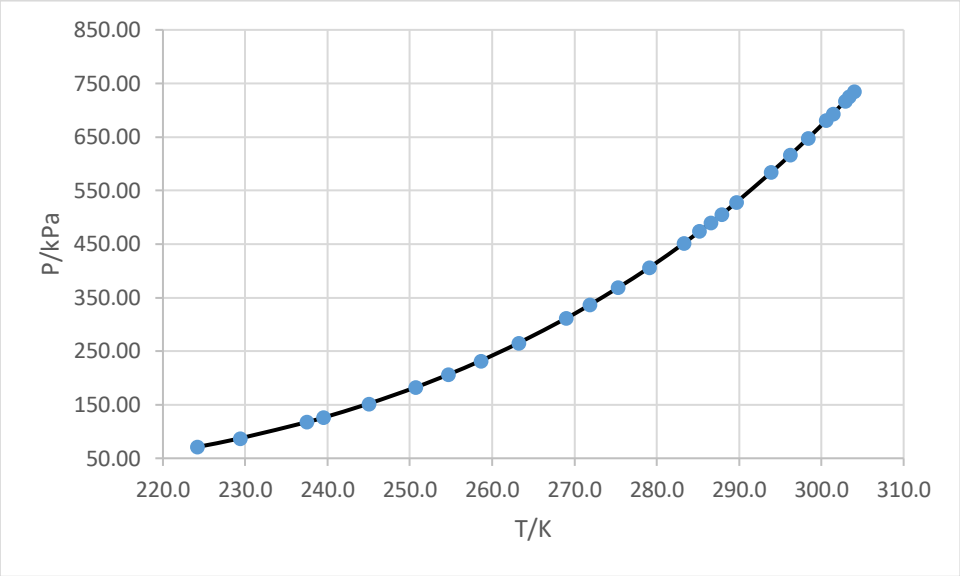

Figure 9 Vapour pressure and temperature data plot for CO_2 (Yaws' Critical Property Data for Chemical Engineers and Chemists
Copyright © 2012; 2013; 2014 Knovel.)

However, a descriptive temperature-independent property of carbon dioxide also tabulated as in *Table 22* in Appendix 1 (Design Institute for Physical Properties, Sponsored,by AIChE a).

4.3 Furfural

Furfural is lignocellulosic biomass derivatives, which thereafter can be processed, to biofuels and biochemicals. The differences in furfural products can be distinguished based on their carbon number and synthesis routes. Those derivatives of furfural can be used to replace fossil fuel-based biofuel and biochemical. Illustrations, *Figure 10* shows below the possible furfural derivatives as fuel components and chemicals (Li, Jia et al. 2016).

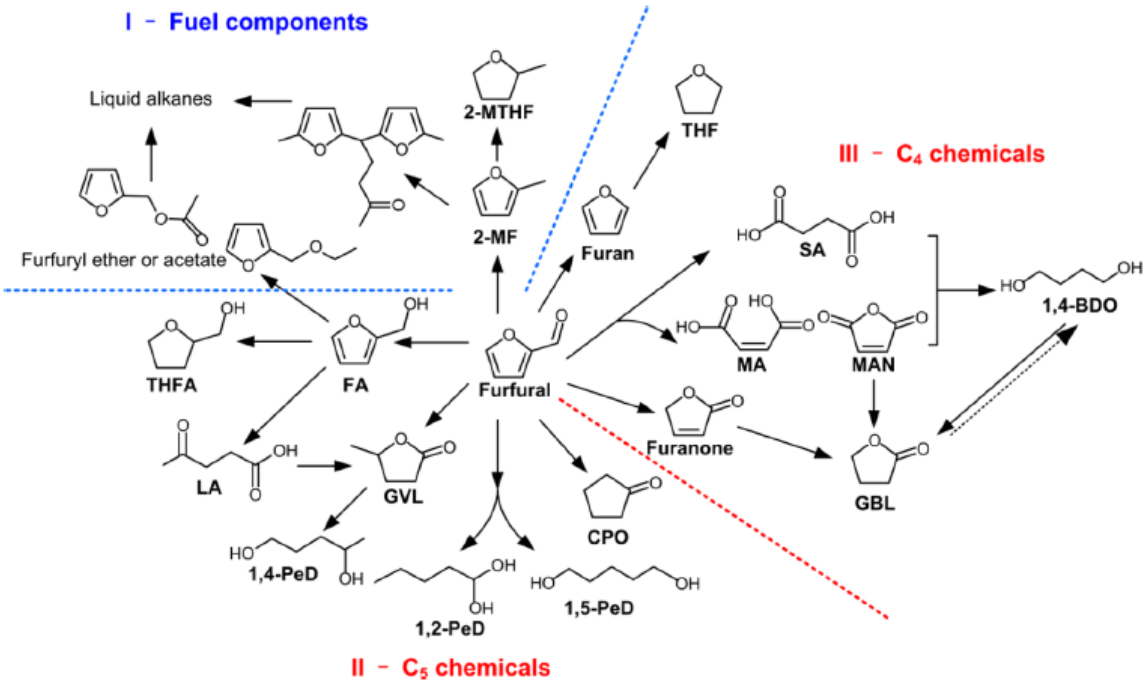

Figure 10: Catalytic conversion of furfural to chemicals and fuel components *(Li, Jia et al. 2016)*

Different furfural derivatives have different applications. For instance, the uses vary from agrochemicals, pharmaceuticals, resins, solvents and so on. In our above-mentioned novel biorefinery process, furfural exists in spent liquor because of wood biomass fractionation. Therefore, the separation of furfural is important to avoid the accumulation of furfural in GVL recycling process. The basic physicochemical properties of furfural can be seen in *Table 2*. The temperature-independent properties of furfural presented below *Table 22* in Appendix 1(Design Institute for Physical Properties, Sponsored,by AIChE b).

Various studies present the furfural vapour pressure data for various temperature ranges. A study conducted by (Fele, Grilc 2003) provides a vapour pressure plot between furfural and furfural derivatives called 5-methyl furfural. However, extracted experimental vapour pressure data carried out by (Riddick, Bunger 1970, Matthews, Sumner et al. 1950) plotted below as *Figure 11* help us to understand the temperature and vapour pressure correlation for our study. The vapour pressure data for furfural is now presented below as *Figure 11*.

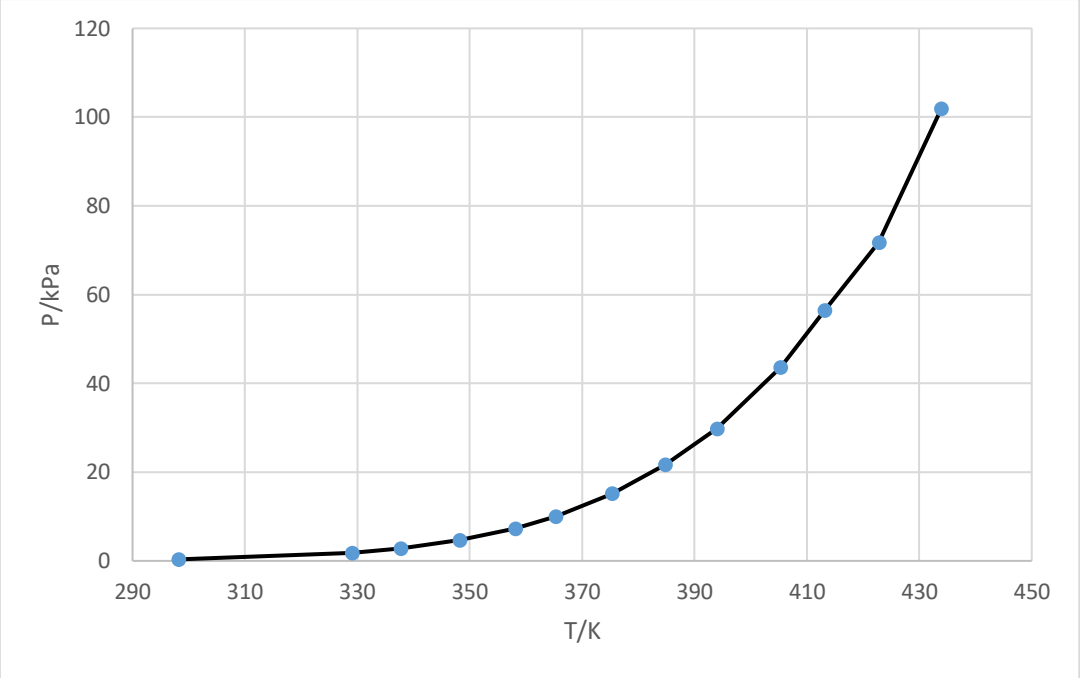

Figure 11: Vapour pressure data of furfural (Riddick, Bunger 1970, Matthews, Sumner et al. 1950)

4.4 Water

Water is also considered as the main component in our thesis work as it exists in real process with large quantity. However, to simplify our thermodynamic modelling, in some simulation stages water has not been taken in count within the system. Therefore, only binary interaction between other components such as GVL and furfural was considered (e.g. vacuum distillation). However, in our liquid-liquid extraction water was taken in count as the main component. The physicochemical properties of water are already presented in Table 2. Here, other temperature-independent properties of water can be found in *Table 22* in Appendix 1.

Here, a vapour pressure graph is also given as in below as *Figure 12*.

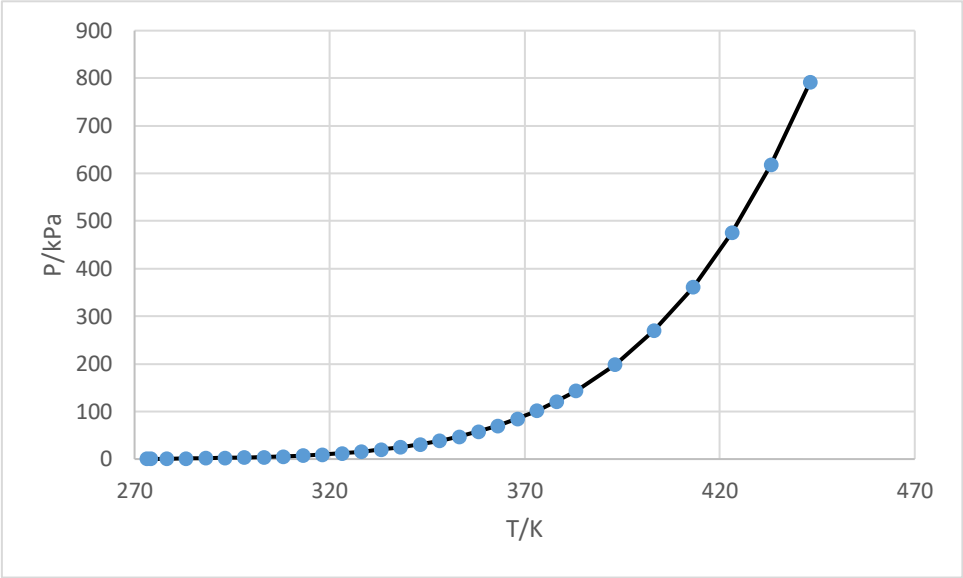

Figure 12: The vapour pressure and temperature diagram of water (Haar, Gallagher et al. 1984)

Further details about the water and its properties can be found in pieces of literature.

5. Thermodynamic Property Methods (Binary systems)

According to the overview of property methods on Aspen-manual book (Anonymous a), unit operation models requires property calculations such as fugacities for thermodynamic equilibrium to generate results. Fugacity and enthalpy are considered as most frequently requested properties and those properties mentioned as the sufficient information to calculate mass and heat balance. However, the quality of property calculation is determined by the model equations themselves and the usage by adding detail information on their property calculation. In the Aspen manual (Anonymous), physical property method discussed as three types such as thermodynamic property method, transport property methods and non–conventional component enthalpy calculation. Non-conventional components are those does not participate in phase equilibrium instead included on enthalpy balance. Here, in this study, it is focused on thermodynamic property methods for calculating the vapour-liquid equilibrium and liquid-liquid equilibrium.

The phase equilibrium calculation is considered as the key thermodynamic property calculation. The equilibrium relationship between two different phases in a process stream

defined with the fugacity of the component in the liquid and vapour phase. The mathematical expression for this basic relationship can be written as an equation below.

$$f_i^v = f_i^l \qquad (1)$$

Where,

f_i^v = fugacity of component *i* in the vapour phase *v*.

f_i^l = fugacity of component *i* in the liquid phase *l*.

There are two methods called as the equation of state and activity coefficient methods are used in applied thermodynamics for representing the fugacities from the phase equilibrium at measurable state variables. The mathematical expression of the equation above in the equation of state method and activity coefficient method can be found in literature such as (Anonymous). The term fugacity and activity coefficient are briefly discussed in section 7.2.

The basis of many separation techniques is phase equilibria. For designing, analysis and control different chemical process system and separation processes require understanding phase equilibrium. For instance, in the distillation process, it requires an understanding of VLE or some cases VLLE as it utilizes the difference between the composition of the vapour and liquid phases occurring in the distillation. Furthermore, for solid-liquid separation or liquid-liquid separation, it requires understanding SLE and LLE behaviour of the components respectively.

5.1 Vapour-Liquid Equilibrium (VLE) theory

In this section, the theory behind the vapour-liquid equilibrium discussed. The equilibrium relationship for any component defined by the K value, which is known as the distribution coefficient. Distribution coefficient, K value is defined as the mole fraction of component *i* in the vapour and liquid phase. Therefore, the K values stand with an equation as,

$$K_i = \frac{y_i}{x_i} \qquad (2)$$

Where, x_i is defined as the mole fraction of component *i* in the liquid phase

y_i is defined as the mole fraction of component *i* in the vapour phase

A term named as relative volatility is used to compare and quantify two components volatility. Relative volatility is the ratio between the distribution coefficients of component *i* and *j*. The term relative volatility comes with an equational expression as (Teja, J Holm 2018),

$$\alpha_{ij} = \frac{K_i}{K_j} = \frac{\frac{y_i}{x_i}}{\frac{y_j}{x_j}} \qquad (3)$$

Where, α_{ij} describes the relative volatility of two components

K_i describes the distribution coefficients of component i

K_i describes the distribution coefficients of component j

The ratio between the two components distribution coefficients defines how the separation efficiency will be. For instance, if the relative volatility values are unity or 1, the more likely it too difficult to conduct separation. Greater or lower values than unity indicate fewer separation stages required to be utilized to carry out the separation in distillation. Extracted data from the literature by (Teja, J Holm 2018) has been plotted which describes the relative volatility as a graph in Figure 13.

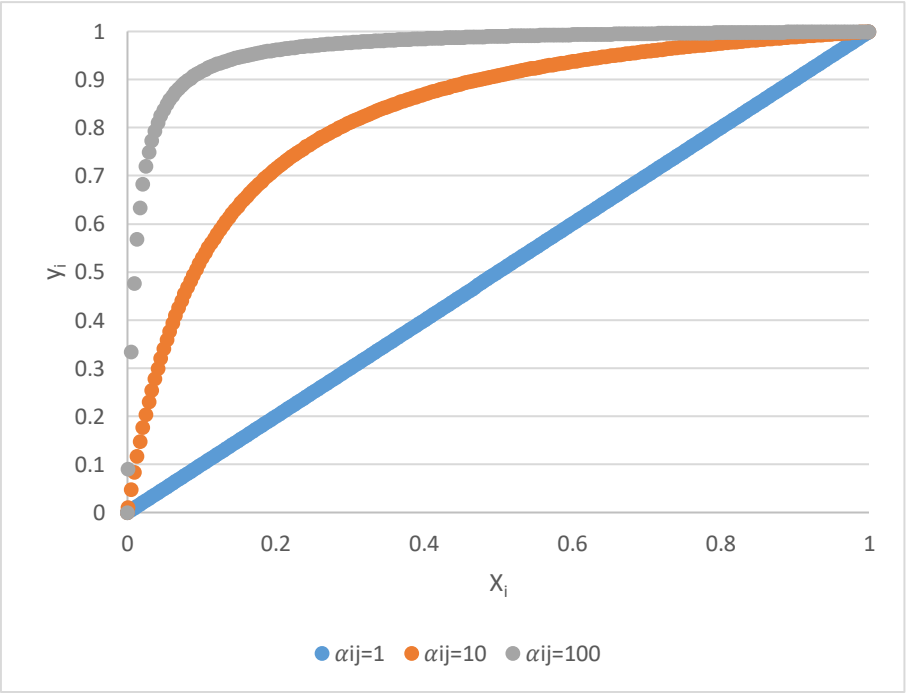

Figure 13: The y-x plot for a binary mixture at a constant temperature for various values of the relative volatility (Teja, J Holm 2018)

According to the plot, when relative volatility α_{ij} is unity, the separation no longer feasible as $x_i = y_i$. The value of relative volatility becomes unity at the azeotropic point. Deviation from 1 on both sides makes the separation feasible and means that few separation stages likely to be required to carry our separation. Therefore, the higher relative volatility leads to an increase of concentration of more volatile components in the vapour phase (Teja, J Holm 2018).

5.1.1 Flash Calculations

According to the book (Smith, J. M., Van Ness et al. 2005) In Vapour Liquid Equilibrium (VLE), the flash calculation is an important application. When the liquid is at equal or greater pressure of its bubble point pressure, its flashes or partially evaporates when the pressure is reduced. Therefore, resulting in it to generate a two-phase system of vapour and liquid in equilibrium. Considering the material balance of a system, where L is referred to be the liquid and V is referred to be the vapour. With a mole fraction of liquid identified as x_i and vapour mole fraction identified as y_i gives the material balance equation for 1 mole as an example given below.

$$6.\quad L + V = 1 \qquad (4)$$

Consider the mole fraction of liquid and vapour gives the equation above a form like,

$$7.\quad Fz_i = x_i L + y_i V \qquad (5)$$

Where, z defines feed composition and subscript $_i$ refer to the number of components in the system, such as (i= 1, 2, ……, N).

By recalling equation above from above Section 5.1 and substituting it into above equation above yields y_i value.

Therefore,

$$y_i = \frac{Z_i K_i}{1+V(K_i-1)} \quad (i= 1, 2, \ldots\ldots, N) \qquad (6)$$

Because, $\sum_i y_i = 1$, equation above is summed overall species to the equation below,

$$\sum \frac{Z_i K_i}{1+V(K_i-1)} = 1 \qquad (7)$$

Therefore, a preliminary step for the calculation of P and T flash problem is to find the value of V. The vapour-liquid x-y diagram can be calculated by setting liquid composition and determine corresponding vapour composition in a bubble point calculation. On the other hand, the vapour composition can be set, and corresponding liquid composition can be determined from dew point calculation (Smith, Van Ness et al. 2005).

7.1 Liquid-Liquid equilibrium (LLE) theory

According to the (Smith, J. M., Ness et al. 2018), VLE is considered to be the most important type of phase equilibrium due to the universality of distillation in the chemical industry. However, few other phase equilibrium phenomena also seek the importance in terms of necessity. Such phase equilibrium phenomena called liquid-liquid equilibrium shortly named as LLE is discussed below. In the book, it was stated that, in the conditions of constant pressure and very low pressure, the binary liquid/ liquid conveniently shows a solubility diagram. According to the (Smith, R. 2005), the separation of two liquids become possible in two phases once the dissimilarity and corresponding activity coefficients becomes large enough. The effect of temperature can be applied to increase or decrease the mutual solubility of the liquid mixture. In terms of liquid-liquid equilibrium, mathematical models such as NRTL and UNIQUAC equations can be used. Parameters from NRTL and UNIQUAC equations can be correlated from vapour-liquid equilibrium data (Gaube 1982a) or liquid-liquid equilibrium data (Gaube 1982b).

A plot of temperature vs the mole fraction shows three types of solubility behaviour. Here below a diagram extracted from (Smith, Ness et al. 2018) described these three types of binary solubility.

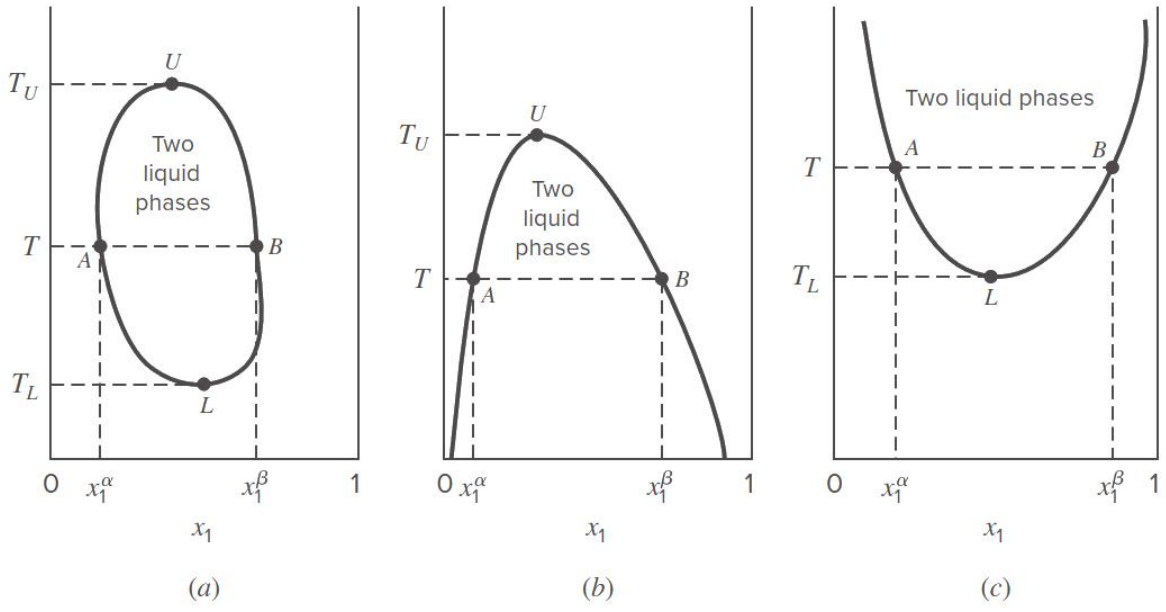

Figure 14 Three types of binary liquid solubility diagram under constant pressure (Smith, Ness et al. 2018)

According to the plot of *Figure 14*(a), it shows the composition of coexisting phases while curve UAL defines the species 2 rich α phase and UBL defines the species 1 rich β phase. The phase equilibrium compositions of x_1^{α} and x_1^{β} at specific temperature T are defined by the intersections of the horizontal line and bimodal curves. Also, the T_L used to define the lower critical solution temperature (LCST) and T_U for describing the upper critical solution temperature (UCST) and those known as consulate temperatures define the limiting states of two-phase equilibrium. Where, in the region between these two consulate temperatures T_L and T_U, liquid-liquid equilibrium can possibly occur. A single-phase is obtained for the full range of compositions while $T < T_L$ and $T > T_U$. At the consulate points, the properties of two equilibrium phases are identical. However, according to the literature, it is rare the view of such behaviour as the liquid-liquid equilibrium binodal curves are often disrupted by curves for yet another phase transition. In the plot of *Figure 14*(b), the behaviour describes the existence of upper critical solution temperature (UCST) during the intersection of the freezing curve. On the other hand, only lower critical solution temperature (LCST) exists when they intersect the vapour liquid bubble point curve. During the intersection of both, no consulate point exists and tend to display another behaviour (Smith, Ness et al. 2018). To calculate the compositions of the coexisting liquid phases for a binary system following equations for phase equilibrium needs to be solved.

$$(x_1\gamma_1)^{I} = (x_1\gamma_1)^{II} \text{ , } (x_2\gamma_2)^{I} = (x_2\gamma_2)^{II} \tag{8}$$

Where,

$$x_1^I + x_2^I = 1 \text{ , } x_1^{II} + x_2^{II} = 1 \tag{9}$$

The given prediction of the liquid-phase activity coefficients from the NRTL or UNIQUAC equations can be used simultaneously to solve the x_1^I and x_1^{II}. According to the literature, there is several solutions to these equations and for a solution to be meaningful:

$$0 < x_1^I < 1 \text{ , } 0 < x_1^{II} < 1 \text{ and } x_1^I \neq x_1^{II} \tag{10}$$

For multi-component systems, the equations to be solved can be found in details on various literature like (Smith 2005). An illustrated Figure 15 The liquid-liquid equilibrium (Smith 2005) extracted from the literature and mass balance equations derivation followed by the figure itself.

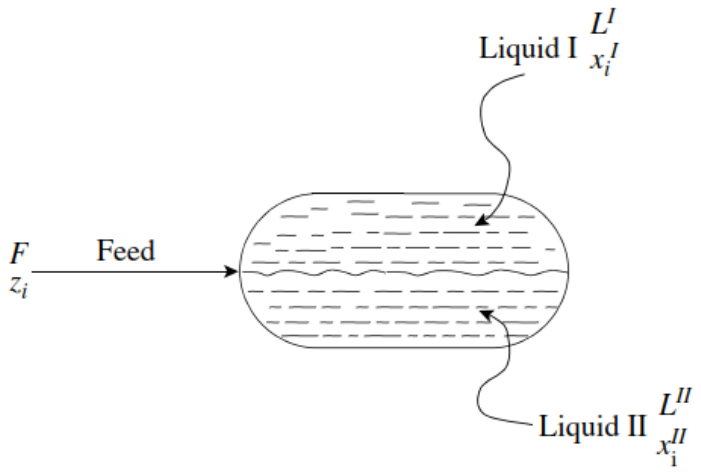

Figure 15 The liquid-liquid equilibrium (Smith 2005)

Where,

F = feed flow rate ($kmol.s^{-1}$)

L^I = flowrate of liquid I from the separator ($kmol.s^{-1}$)

L^{II} = flowrate of liquid I from the separator ($kmol.s^{-1}$)

z_i = mole fraction of component I in the feed

x_i^I = mole fraction of component I in the liquid I

x_i^{II} = mole fraction of component I in the liquid II

Obtained results from the mass balance equation can be applied to solve the equations, 8-10 above. Here below, the mass balance equation for the two liquid phases is given (Smith 2005).

$$\sum_i^{NC} \frac{z_i(K_i-1)}{\frac{L^I}{F}(K_i-1)+1} = 0 = \int(\frac{L^I}{F}) \qquad (11)$$

$$K_i = \frac{x_i^I}{x_i^{II}} = \frac{\gamma_i^I}{\gamma_i^{II}} \qquad (12)$$

where,

K_i = distribution coefficient for component i

Simultaneous variation of x_i^I, x_i^I ……., x_{NC-1}^I and x_i^{II}, x_i^{II}……, x_{NC-1}^{II} and $\frac{L^I}{F}$ solves the equations 11-12 above.

7.2 Fugacity in mixtures

Fugacity is considered to be the central property in phase equilibrium (Matsoukas 2013). According to the literature (Rarey, Gmehling et al. 2012), the behaviour of the real fluid or fluid mixture can be described by means of the fugacity. Determination of fugacity of a species in a mixture is like the pure component fugacity. In the book, the mathematical expression of fugacity of pure component is given. Here below, the extracted equation is given.

$$\overline{g_i}\ (\mathrm{T}, \mathrm{P}, x_i) = g_i^{Pure}(\mathrm{T}, P^o) + \mathrm{RT}\ \ln \frac{f_i}{f_i^0} \qquad (13)$$

where, $g_i^{Pure}(T,\ P^o)$ describes the Gibbs energy of the pure component at the system temperature and randomly chosen temperature P^o. In addition, the fugacity coefficient of a species in a mixture is also defined similarly of fugacity coefficient of a pure component but different in structure. The difference is total pressure replacement by partial pressure. However, the details of the determining the fugacity coefficient, fugacity of ideal mixtures and uses of fugacity coefficient in phase equilibrium is well described in the book (Rarey, Gmehling et al. 2012).

7.3 Mass and Energy Balance

During process calculation, it is important to continue with mass and energy balance. According to (Matsoukas 2013), mass is a conserved quantity, which explains that all the mass crosses the boundaries of a system must be considered. The general mass balance equation below is given below.

$$\text{Mass (in)} - \text{Mass (out)} = \text{Mass (accumulation in the system)} \qquad (14)$$

The balanced equation for mass is applied at all time even with a small-time interval (*dt*). in terms of dynamic simulation. Other special cases such as closed system and steady state can be considered prior to the equation construction. During the mass balance of the system, it is important to know about the exchanges that cross the system boundaries where internal details are insignificant. At steady state, the accumulation is zero which means mass enters to the system will be resulting in a similar output.

In terms of energy balance, it follows the same general balance equation of mass balance. Where it can be as below:

$$\text{Energy (in)} - \text{Energy (out)} = \text{Energy (accumulation in the system)} \qquad (15)$$

Before constructing the energy equation, it is important to define all the exchanges of energy between the system and surroundings. In the process industry, the flow may transfer heat as energy form to surroundings or receive from surrounding and shaft work. There are few possibilities explained which might allow heat exchange such as heat exchanger, shaft work can be exchanged in pumps, compressor and so on. The total amount of heat exchanged, and the total amount of shat work done is described by using $\dot{Q}$ and $\dot{W}_s$ respectively. Also, the calculation of heat exchange and shaft work done is carried out over a time interval (*dt*). Therefore, the mathematical expression of those terms can be written as below.

$$\text{Heat and shaft work in} = \dot{Q}dt + \dot{W}_s\, dt \tag{16}$$

However, the positive and negative sign conventions are used to define the energy entering or exiting respectively. Since, the energy carried out by mass in different forms such as kinetic, potential and internal energy. The mass (*dm*) carried combined energy of different forms over a time interval (*dt*) can be expressed in the mathematical form below.

$$\frac{v^2}{2}\, dm + \text{gz}\, dm + \text{U}\, dm \tag{17}$$

The first term of the equation above describes the kinetic where the velocity of the fluid involved, the second term stands for the expression of potential energy due to gravity and the final term describes the internal energy. However, any other external work carried out to push fluid which contributes to the system need to consider during constructing the balance equation. The more detailed calculation and description can be found in textbooks and different literature sources such as (Matsoukas 2013).

8. Thermodynamic Models

In this section of literature, it was generally discussed the thermodynamic models associated with this study. In terms of choosing the thermodynamic models appropriate for our thesis case study, the guidance from thesis instructor and literature were used. A thermodynamic model tree chart from literature was used to carry on applying thermodynamic models for our study. However, as those mathematical terms and functions were in-built in Aspen plus simulation software, less focus on the derivation of equations were considered. Therefore, a brief discussion on using those thermodynamic models was considered here. Here below, a logical

procedure for choosing a thermodynamic model given as chart was extracted from online literature (Elliott, J. Richard,, Lira,Carl T., 2012).

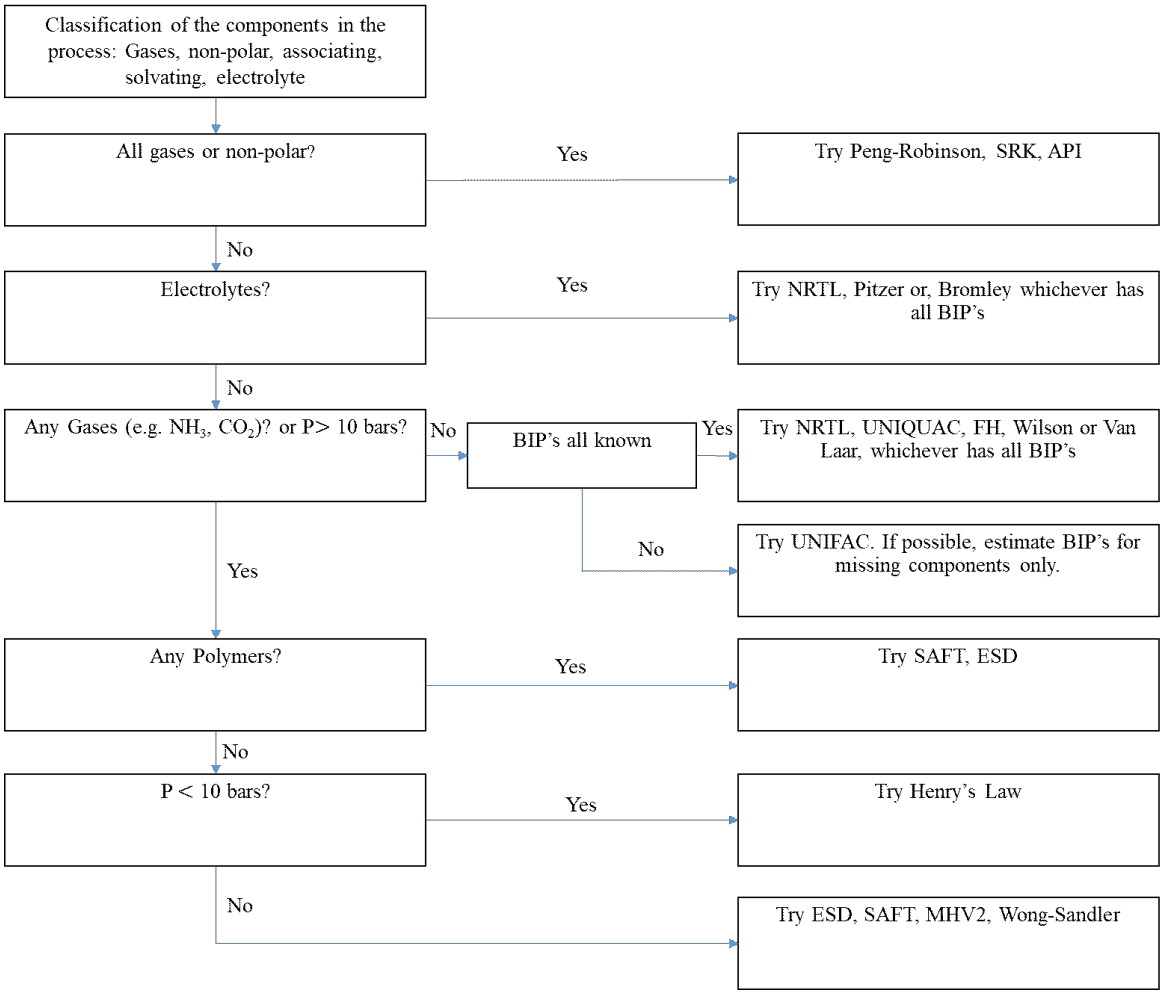

Figure 16: Extracted flow chart of selecting a thermodynamic model. Here, BIP's defines the binary interaction parameters in the diagram (Elliott, J. Richard,, Lira,Carl T., 2012).

However, our study contains different type's components such as gases and liquids and several steps of chemical processes. Therefore, during the simulation in terms of avoiding complexity, it was considered different thermodynamic model types in different steps of the entire process within-study scopes. Therefore, different thermodynamic models applied instead of using the individual uniform thermodynamic model for the entire process. Here, below briefly described the applied thermodynamic models for our study.

8.1 Modified UNIFAC Dortmund

The formation of UNIFAC solution of groups model is based on the extension of a model known as the quasi chemical theory of liquid mixtures in shorten named as UNIQUAC model. According to the UNIFAC model, it progresses through the estimation of the activity coefficients in non-ideal liquid mixtures. Where the methods combine the solution of functional groups concept with a model for activity coefficients based on UINQUAC method extensions. As a result, the UNIFAC model contains two adjustable parameters for every pair of functional groups attached (Fredenslund, Jones et al. 1975). According to the same literature, the advantages of the UNIFAC model is, it can utilize the existing phase equilibrium to predict the phase equilibria of the system which has no experimental data available. The concept of the UNIFAC model follows the ASOG model where activity coefficients in mixtures are related to structural group's interactions. Therefore, the application of the UNIFAC model can be used to reduce the generation of activity coefficients data experimentally which are required to obtain the parameters to characterize the structural group's interaction in nonelectrolyte systems. Also, to predict the activity coefficients of another system which exists with the same functional groups.

However, the original UNIFAC model can be used to predict the vapour-liquid equilibria (VLE) and azeotropic data, where the major modification brought into the modified version of UNIFAC that, it can also predict some other systems such as solid-liquid equilibria (SLE) of eutectic systems, liquid-liquid equilibria (LLE), excess enthalpies (h^E), activity coefficients at infinite dilution (γ^∞). The comparison between original UNIFAC and modified UNIFAC is well described in the literature titled with A modified UNIFAC model. 1. Prediction of VLE, h^E, γ^∞ (Weidlich, Gmehling 1987). To overcome the limitations in original UNIFAC model such as the possibility of leading poor results in predicting the real phase behaviour of systems for mixtures at high temperature (>400K) and low temperature (<290K). The major development has been made in the modified UNIFAC model is in their combinatorial part to improve the results for the asymmetric system where molecules are varied differently in sizes and shapes. In addition, temperature-dependent of parameters were introduced to define relations between the activity coefficients as a function of temperature accurately (Lohmann, Joh et al. 2001). How the parameters of the temperature-dependent interaction differentiate the modified UNIFAC model from the original UNIFAC is described in equations here below (Gmehling, Lohmann et al. 1998).

The original UNIFAC model:

$$\psi_{nm} = exp\left[-\frac{a_{nm}}{T}\right] \quad (18)$$

The modified UNIFAC Dortmund model:

$$\psi_{nm} = exp\left[-\frac{a_{nm} + b_{nm} + c_{nm}T^2}{T}\right] \quad (19)$$

Where, ψ_{nm} is defined as the UNIFAC/ modified UNIFAC Dortmund temperature term. In addition, a_{nm}, b_{nm}, c_{nm} defines the UNIFAC group interaction parameters between main groups n and m.

The reliability of temperature dependency of the modified UNIFAC Dortmund model group interaction parameters is maintained by the help of Dortmund Data Bank (DDB) by enabling accessing collection of thermodynamic mixture data at different temperature ranges by temperature extrapolation. Therefore, the modified UNIFAC- Dortmund group contribution model is applied in various industrial interests, where it's provided with a reliable and better estimation of real phase behaviour and helps the calculation of chemical equilibria, K = $\frac{K_x}{K_y}$ and flashpoints. The more detailed advantages of modified UNIFAC Dortmund well described in various literature (Lohmann, Joh et al. 2001, Gmehling, Lohmann et al. 1998).

8.2 KLL correlation

In terms of calculating the liquid-liquid equilibrium K-values (distribution coefficients), it can be used Extract, RedFrac and Decanter in unit operation models. The liquid-liquid equilibrium behaviour of the extraction process can simulate using the built-in KLL expression in Aspen Plus. According to the Aspen Plus, when calculating the liquid-liquid distribution coefficients (KLL), by using default decanter, it uses the physical property method. A decanter can perform the liquid-liquid distribution coefficients (KLL) using different thermodynamic models such as activity coefficient model, an equation of state capable of representing two liquid phases, a user-specified Fortran subroutine and a built-in correlation with user-specified coefficients. While, using default decanter, on the input and calculation options sheet, it is possible to override the default by specifying the separate property methods for two different liquid phases or use a built-in KLL correlation or use a Fortran subroutine in KLL subroutine sheets.

However, the built-in KLL expression is given in Aspen Plus and other literature as given below(Aspen Technology b, Aspen Technology a, Anonymous b).

$$ln(K_{LL}) = a + \frac{b}{T} + c.ln(T) + d.T \qquad (20)$$

Where,

K_{LL} = is the liquid-liquid equilibrium K-value (partition ratio)

a, b, c, d = regression coefficients parameters

T = temperature in K

8.3 Soave -Redlich Kwong (SRK) Method

In this section, It is discussed the general background of the Soave -Redlich Kwong or shortly known as SRK method in the field of calculation the thermodynamic behaviour. The Soave -Redlich Kwong models are classified as the equation of state (EOS) models, where an equation of state stand as a semi-empirical functional relationship between the pressure, volume and temperature of a pure substance. The basis of various equation of state models comes from the Van der Waals Equation of state. The Equation of State (EOS) thermodynamic models describe the state of matter in a given set of properties. However, in terms of a multi-component system, it requires additional variables e.g. composition to produce appropriate mixing rule (Ramdharee, Muzenda et al. 2013).

The mathematical expression of EOS is written as below in the literature,

$$f(P, V, T, a_k, K = 1, n_p) = 0 \qquad (21)$$

Where the a_k and n_p defined as the EOS's parameters and categories. It was stated in the literature that, the complexity of n_p defines the accuracy of EOS. Higher accuracy comes with the complexity of n_p term. In terms of predicting the thermodynamic properties more accurately for all substances under different conditions requires multiple equations (Salehpour, Dubé 2008).

The SRK model was the result of an important notification to the Redlich-Kwong Equation of State (EOS), which was proposed by Soave in 1972. The major improvement to the Redlich-Kwong Equation of State (EOS) enabled it to predict the phase behaviour of the mixture in the critical region and fitted the vapour-liquid data well to the model. According to the review article of (Ramdharee, Muzenda et al. 2013) which extracted the statement from (Advantages of

Using Cubic Equations of State; Phase Relations in Reservoir Engineering) that, Soave proposed the two variables dependency instead of focusing only temperature dependency of the attractive parameters in Van der Waals equation of state. In his proposal, it was included the shape of molecules through the Pitzer's acentric factor ω. Therefore, the two variable dependencies for "a" is described below as equation

$$a = a\,(T,\omega) \qquad (22)$$

Although SRK method is capable of predicting both vapour and liquid phase behaviour, it has some drawbacks such as estimating, molar volume and densities as a result from accounting the unrealistic universal critical compressibility value of 0.333 for all substances. The mathematical expression for SRK EOS and detailed descriptions are given in many kinds of literature and can be found for instance in (Aasen, Hammer et al. 2017, Ghasemian, Kalbasi et al. 2013). To improve its accuracy many modifications were suggested. According to (Ramdharee, Muzenda et al. 2013), the equations are given as below.

$$P = \frac{RT}{(V-b)} - \frac{a\,\alpha}{V(V+b)} \qquad (23)$$

Where α correlation

$$\alpha = [1+ S\,(1-(T_r)]^2 \qquad (24)$$

In addition, the value of S can be calculated from the equation below, S

$$S = 0.48 + 1.574\omega + -0.176\,\omega^2 \qquad (25)$$

In equation 23 above, V defines the molar volume and b is the co-volume. Reduced temperature defined as T_r.

9. Liquid-liquid extraction & liquid CO_2

According to the literature (Berk 2013), liquid-liquid extraction is a mass transfer driven separation process, transfers solute from one solvent to another while two solvents are completely or partially immiscible to each other. The mode of operation and selection of solvent plays an important role in terms of defining the separation efficiency while one solvent is usually aqueous and other is non-polar solvent. Followed by other extraction processes, liquid-liquid extraction also follows the same step of phase separation. The phase equilibrium

reaches when the extractable solutes reach to equal in the amount in two phases and defined by the distribution coefficient K as follows,

$$K = \frac{C_1}{C_2} \qquad (26)$$

Where C_1 and C_2 describe the equilibrium concentration of solute in two phases. It was stated (Männistö, Pokki et al. 2018) that, in terms of selecting solvents, their boiling points are considerably higher and lower than the desired chemical needs to be extracted. By operation principle, extract requires further employment of separation process such as distillation to separate the desired chemicals from. It implies that the separation is based on the distribution of desired chemical and both organic and aqueous phase and can be assessed by measuring the liquid-liquid equilibrium between selected components. During the liquid-liquid extraction, desired chemical or solute preferentially partitions from diluent due to its higher solubility compared to the solubility of diluent with extractants. An illustrated graphics of liquid-liquid extraction process highlighting its concentration profile is given below as *Figure 17*.

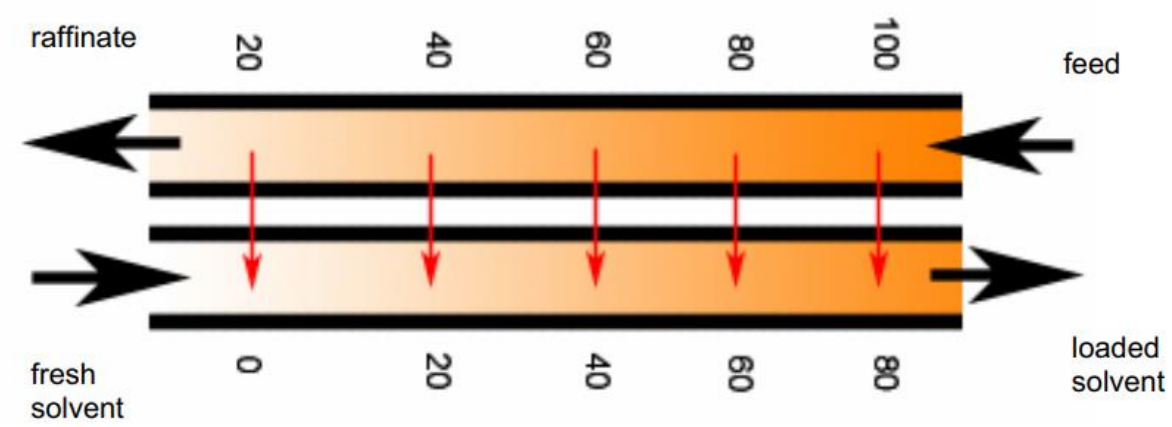

Figure 17. Counter-current multistage liquid-liquid extraction process with concentration profiles (Law, Todd 1.12.2008)

Assuming each stage involved in the extraction process is ideal and total balance equation for the first stage can be expressed as given as below

$$F + E_2 = R_1 + E_1 \qquad (27)$$

Where, F = feed, E = extract, R = raffinate and subscript number describes the position of the stage.

If the extraction process involves a number of components and can be described as component *i* and *j*. For instance, the component balance for the component '*i*' is,

$$F x_{F,i} + E_2 x_{E_2,I} = R_1 x_{R_1,I} + E_1 x_{E_1,i} \qquad (28)$$

Also, the total balance for stage 'n' can be written as,

$$R_{n-1} + E_{n+1} = R_n + E_n \qquad (29)$$

The component balance for the component I on n^{th} stage expressed as,

$$R_{n-1} x_{n-1,i} + E_{n+1} x_{E_{n-1,i}} = R_n x_{Rn,i} + E_n x_{En,i} \qquad (30)$$

Followed by, the last stage total balance,

$$R_{n-1} + S = R_n + E_n \qquad (31)$$

Accordingly, the component balance for the component '*i*' would be for the last stage as follows,

$$R_{N-1} x_{N-1,i} + S_{x_{s,i}} = R_n x_{R_{N,i}} + E_n x_{E_{N,i}} \qquad (32)$$

Therefore, every stage in operation generates 4 balance equation for the ternary system (Pokki 2017).

The application of liquid-liquid extraction can be found in various sectors such as chemical, pharmaceutical, petroleum, nuclear and food industries (Lestari, Salari et al. 2016). In addition to this liquid-liquid extraction advantages over the distillation process by avoiding the energy-intensive process of liquid evaporation and enabling separation of azeotropic mixtures (Stahl, Schuetz et al. 1980).

The uses of carbon dioxide as solvents in its supercritical form or as liquid form is well established. Uses of supercritical fluid extraction using CO_2 has many advantages over many other solvents in terms of its various properties such as CO_2 natural abundance, non-toxic, non-combustible, odourless, tasteless, higher diffusivity and so on. However, sometimes liquid CO_2 makes a selection over supercritical CO_2 in many scenarios. It was found that many organic compounds are more soluble in liquid solvents than the supercritical CO_2 (Phelps, Smart et al. 1996). Perhaps, this advantage may not relate our study scenarios where energy consumption is more concern. As reaching the supercritical phase of CO_2 by manipulating the pressure and temperature would require high energy allows liquid CO_2 over supercritical CO_2. In addition, it was also found that liquid CO_2 is intrinsically not different than supercritical CO_2 despite

some physical properties dissimilarity (Hyatt 1984). A density profile of CO_2 as a function of pressure and temperature is given below *Figure 18*.

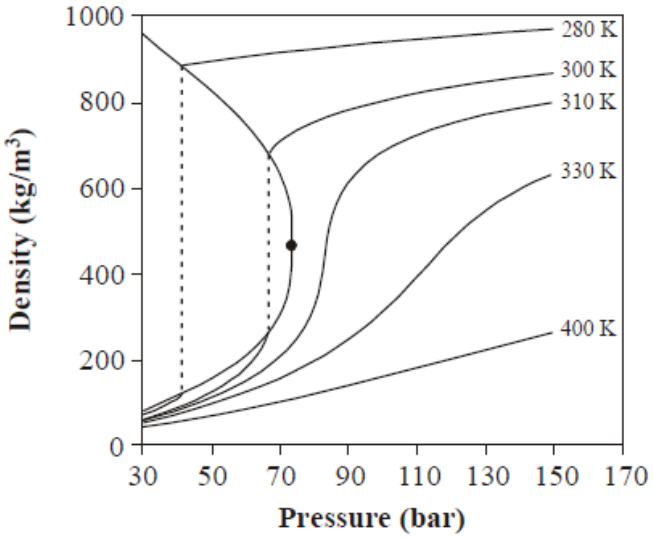

Figure 18. Illustration of carbon dioxide pressure density diagram (Sapakale, Patil et al. 2010)

Here the diagram provides the density information of liquid carbon dioxide at temperature and pressure ranges.

7.2 Compressibility factor of CO_2

The understanding of carbon dioxide behaviour is important as in our system we are focusing on recycling carbon dioxide. During compressor design, it is therefore required to use precise density, viscosity and phase behaviour data of carbon dioxide. As it was previously mentioned that, carbon dioxide has a low critical temperature. Therefore, technically it can be easily transported through the pipeline as gas or supercritical fluid or as subcooled liquid based on the pipeline system temperature and pressure. However, it is important to maintain a lower saturation state by reducing water content from the system by more than 60% if the process involved a water component. In terms of intercooler compression, moisture can be removed by condensation. Before reaching to final compression stage, it is required to carry on further drying since moist carbon dioxide is highly corrosive medium. To eliminate the issues related to corrosion, stainless steel materials can be used.

The aspects such as system process design, pressure losses, mechanical construction, energy and cost-efficiency of the process are determined by the method of controlling temperature and

under particular conditions. According to literature (McCoy, Rubin 2008), the nonlinear compressibility of carbon dioxide in the range of pressures common for pipeline transport which was predicted by using the Peng-Robinson equation of state.

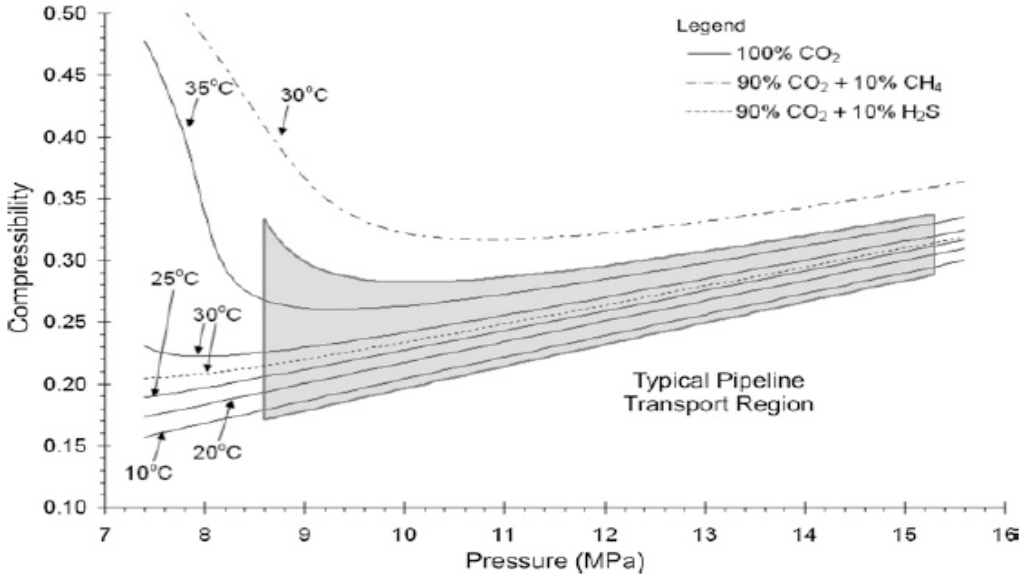

Figure 19: Nonlinear compressibility of carbon dioxide in the range of pressures common for pipeline transport (McCoy, Rubin 2008)

According to (McCoy, Rubin 2008), it was recommended to operate the carbon dioxide pipeline at 8.6 MPa to avoid impact due to dramatic changes in temperature and reduce difficulties during design and operation. However, considering the pressure drop and appropriate pipeline distance effects pressure values and require compressors higher discharge pressure.

10. Vacuum Distillation

In chemical process industries use of the distillation process is the most common scenario. Distillation usually carried out by separating mixture components with volatility differences in their liquid and vapour phase. To continue the separation process, external energy such as heat is provided to generate the phase change from liquid to vapour which initiates the mole fraction difference of a component in the liquid and vapour phase. Prior to the distillation process, it is important to define operating conditions such as temperature, composition, pressure, number of stages, column configuration and so on. However, at the initial stage of modelling we carried out work with assumptions such as some factors like pressure, column configuration and so on

are fixed, where main factors temperature and composition requires main attention. From above mentioned two main factors, temperature plays a predominant role (Khoury 2014). In this section, the binary distillation process principle was approached only due to process simplicity which allows simulating the distillation process using a simplified model. In our system, the GVL is recovered at the last stage from furfural, where distillation column is introduced to separate two components from each other. The distillation column itself consists of plates or stages where the equilibrium between vapour and liquid takes places. It is based on an assumption that the vapour and liquid leaving the same stage is in equilibrium condition (Teja, J Holm 2018). A chemical process with multicomponent mixture during distillation process distributes the components in both vapour liquid phase in equilibrium. In addition, at the initial stage, the binary system helps good understanding of approximation for the multi-component separation. Although, in real life, the binary system is not common as the chemical process industry deals with multi-component mixture or system exist with various impurities. Here below a schematic of a distillation column is presented.

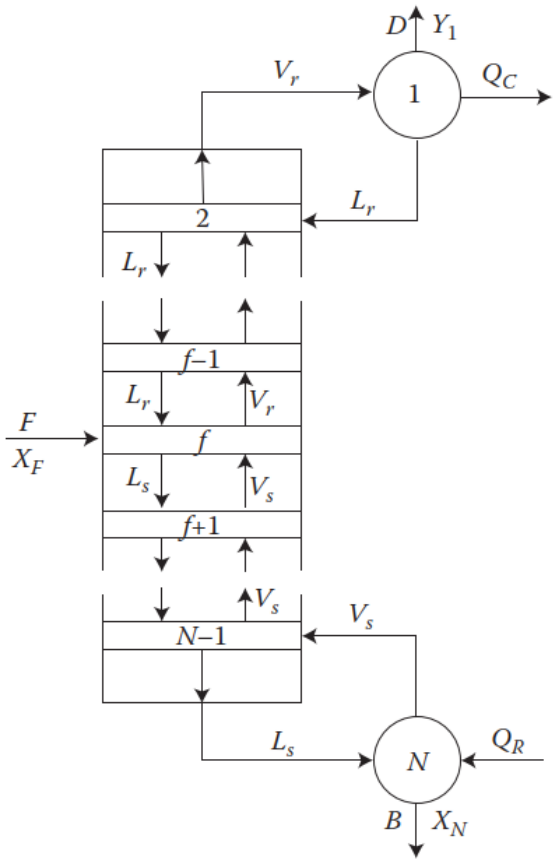

Figure 20. Schematic of a distillation column (Khoury 2014)

According to the literature, a typical distillation column is built with one feed stream. On the overhead of the column releases the top distillate and bottom of the column release bottom distillates. Its operation principle explains that vapour rising from the top of the columns gets partially condensed, the vapour and liquid are separated. The vapour is taken out as distillate at its dew point and liquid is returned back to the column section as reflux. However, in partial condensation stage account as a stage, one or additional equilibrium stage as there both vapour and liquid interact with each other. Therefore, the column top tray is stage 2 and so on.

A component balance representation in the column section is given below by a schematic extracted from the source (Khoury 2014).

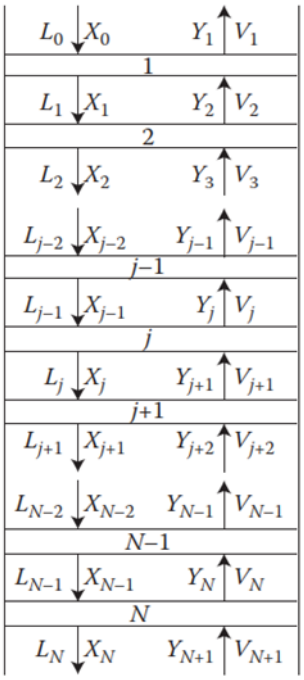

Figure 21. Schematic of column section (Khoury 2014)

According to the column section schematic above, the column section itself contains N number of equilibrium stage designated by the subscript j. Also, the liquid and vapour molar flow rate is described by the L_j and V_j. Mole fractions of more volatile components for the L_j and V_j designated by Xj and Yj respectively. Therefore, the column section can simultaneously be solved by the simultaneous solution of the component mass balance equations and vapour-liquid equilibrium relations. Here an example of the component balance equation on the most volatile component is given.

$$L_{j-1}X_{j-1} + V_{j+1}Y_{j+1} = L_jX_j + V_jY_j \qquad 33$$

The equilibrium relation on equilibrium stages expressed in mathematical form as

$$Y_j/X_j = K_{j1} \qquad 34$$

and

$$(1-Y_j)/(1-X_j) = K_{j2} \qquad 35$$

However, the details about many other parameters, calculations and operating principles can be found in the literature (Khoury 2014). Before, heading to rigorous calculation, a graphical solution can be useful approximating the number of stages which therefore can be the basis of mathematical of software simulation. McCabe-Thiele method is a useful graphical solution of binary distillation on a Y-X diagram (Mccabe, Thiele 1925). A representation of the McCabe-Thiele diagram is given below.

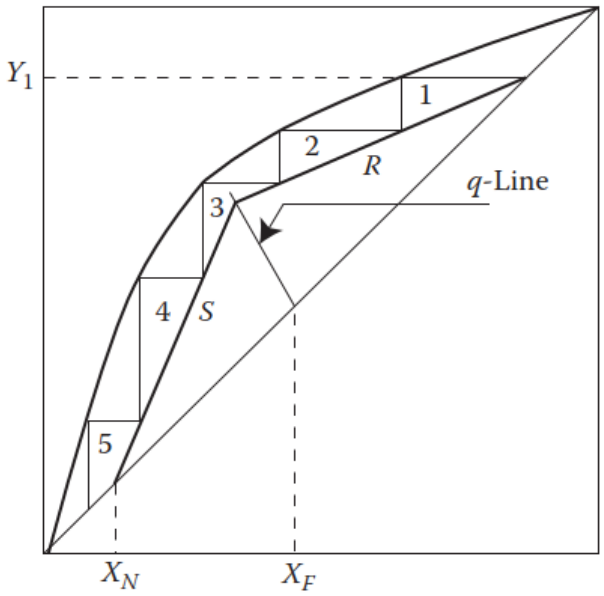

Figure 22. Schematic of McCabe-Thiele diagram (Khoury 2014)

According to the figure above, a phase equilibrium data is first plotted on a Y-X diagram and therefore, The operating lines, assumed straight lines, are then plotted on the basis of known points, slopes, and/or a number of stages, depending on which variables are specified. These give approximate data of stages only. However, the q line depends on the feed thermal conditions. Another figure below represents, the q-line drawing on different feed thermal conditions.

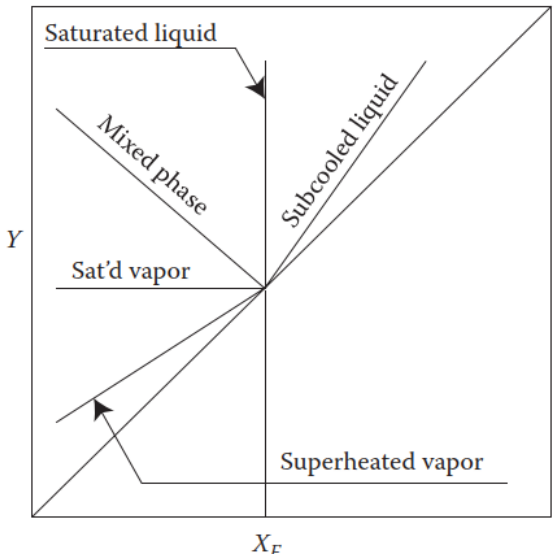

Figure 23. The schematic of q-lines for different feed conditions (Khoury 2014)

Further details of q-line operation can be found on many kinds of literature such as (Khoury 2014).

The q line slope data is given below (Khoury 2014).

Feed thermal condition at	T_f, P_f	q**-Line slope**
Superheated vapor	$q < 0$	$0 <$ Slope < 1
Saturated vapor	$q = 0$	0
Mixed phase	$0 < q < 1$	$-\infty <$ Slope < 0
Saturated liquid	$q = 1$	∞
Subcooled liquid	$q > 1$	$\infty >$ Slope > 1

Simulation and Calculation

In this chapter, it will be discussed the simulation work carried out for our study accordingly. It has been mentioned in the earlier chapter of section 2 that, our study aimed to carry out a distillation process for GVL solvent and furfural. However, every stage was carried out separately instead of a using single uniform thermodynamic model based on their feed conditions, state of the components and process simplicity.

11. Simulation of vacuum distillation

In this section, it is discussed the vacuum distillation of GVL and Furufural system. Here below, all findings are tabulated. There are two different case study carried out for the separation of GVL and furfural. The section below 9.1 to 9.4 contains case study 1 and section 9.5 focused on only using vacuum distillation column and case study 2 for separating GVL and furfural using stripping column with distillation column.

9.1 Vapour liquid equilibrium of GVL and Furfural:

According to the block diagram in the earlier section 2, the last part of the process involves the vacuum distillation of GVL and furfural. VLE diagram of the GVL and Furfural were generated using Aspen simulation software.

Using the UNIFAC-Dortmund method in Aspen Plus simulation software provided the vapour-liquid equilibrium plot of the GVL and Furfural. The phase equilibrium curve is presented below as *Figure 24*. Here, in the plot, GVL and Furfural described as GAMMA-01and FURFU-01 respectively.

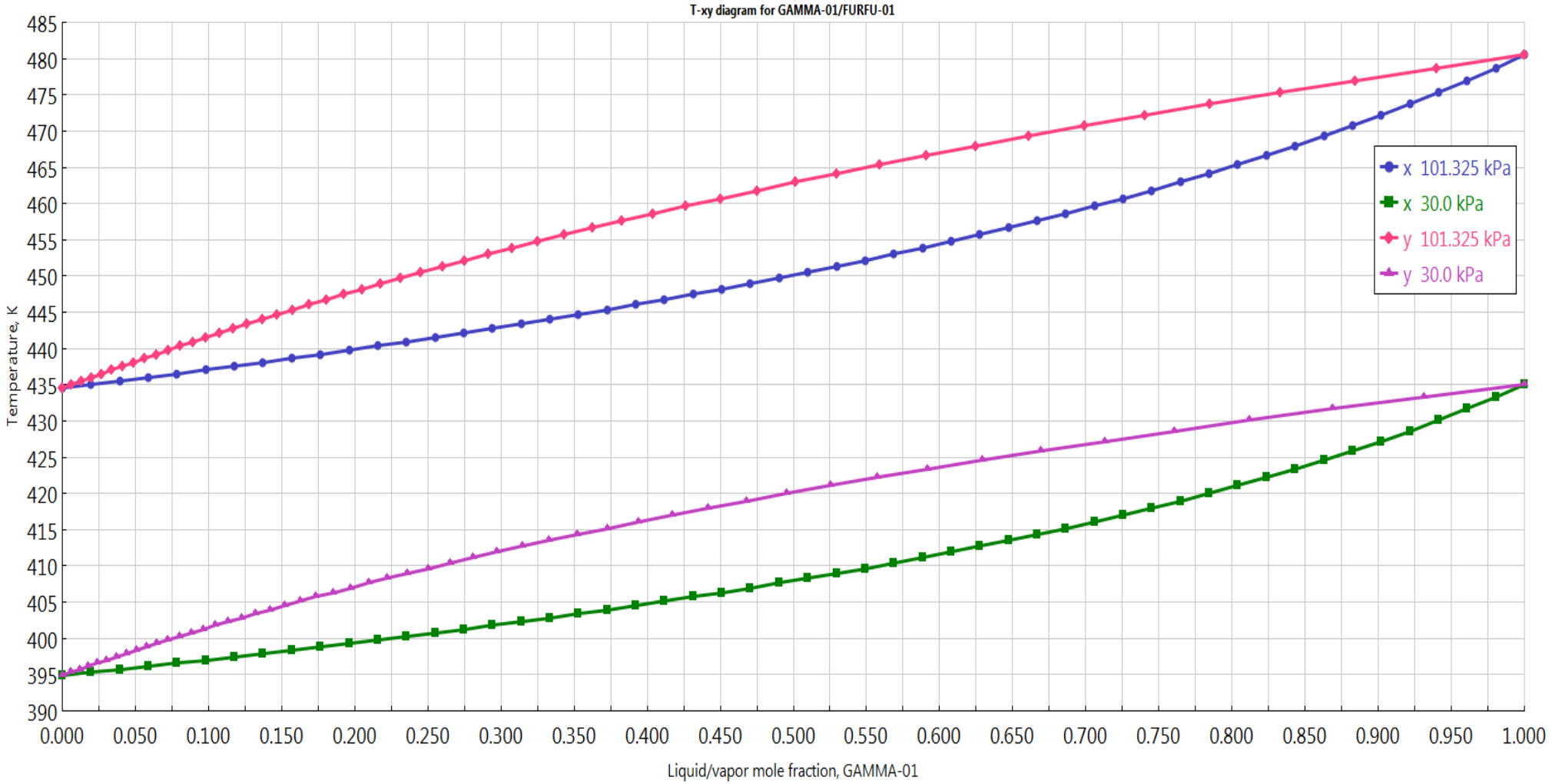

Figure 24. T-xy Diagram of the GVL at pressure 101.325 kPa and 30 kPa

1

Where *x* and *y* represent the liquid mole fraction and vapour mole fraction of GVL respectively.

According to the plot above in *Figure 24*, it can be seen that in the given temperature range it does not create azeotropes, which indicates the possibility of separating both GVL and furfural as pure components theoretically.

9.2 Theoretical stages and minimum reflux ratio

To determine the minimum number of theoretical stages and minimum reflux ratio of the distillation process, assumptions of the molar feed rate of both GVL and furfural in the feed stream given below as *Table 4*.

Table 4: Feed composition and individual feed rate used in a distillation column

Remarks	Composition	Feed rate	Units
$z_{furfural}$	0.05	2072	mol/hr
z_{GVL}	0.95	39370	mol/hr
Total feed	1.00	41442	mol/hr

The assumption of individual feed and total feed amount was based on the prior study carried out as part of the doctoral study (Lê, Pokki et al. 2018). It was assumed the mole fraction of furfural in feed is 5.0% where the rest of the feed contains GVL. Thereafter, the feed line, stripping line and rectifying line has been drawn in the plot to calculate the number of minimum theoretical stages and minimum reflux ratio. In addition, the q-line values were decided was close to $0.99 < 1$ based on feed thermal state.

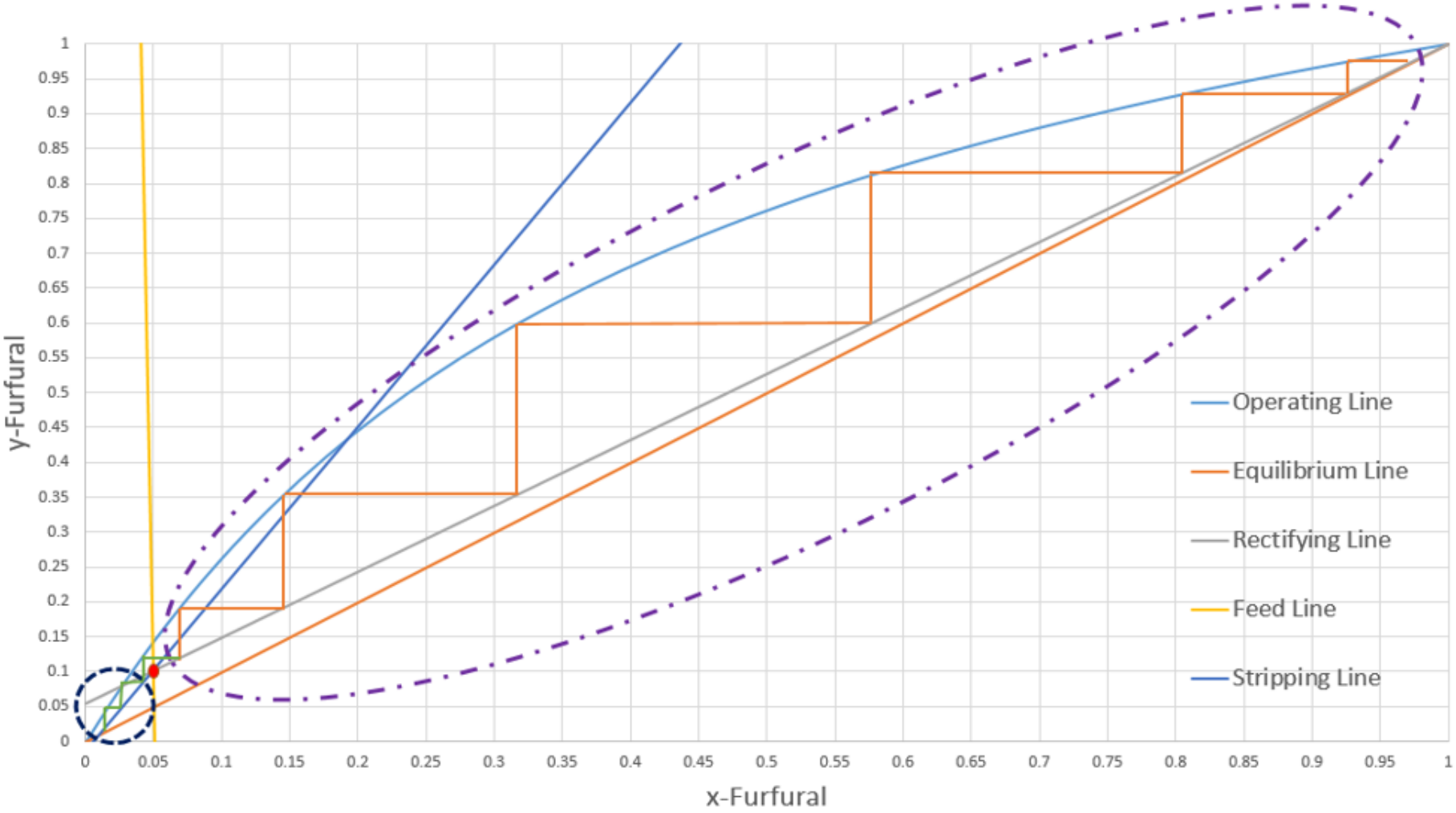

Figure 25. Mc-Cabe Thiele diagram of theoretical stages for GVL and furfural distillation.

According to the Mc-Cabe Thiele graphical plot *Figure 25*, the most volatile component which is going to be collected from the top of the distillation column required to be drawn in the plot. In the plot, it can be seen that liquid mole fraction and vapour mole fraction are considered as x and y respectively. For the given composition of GVL and furfural, estimated results are given below as *Table 5*.

Table 5: Estimated results from McCabe-Theile diagram for given GVL/Furfural composition

Minimum Reflux	8.7
Estimated Reflux	15
Total No. of stages	9
Rectifying stages	6
Stripping stages	3

However, it was suggested that, in practice operation of distillation, the number of theoretical stages better to apply double in a number of the minimum. Therefore, the total number of theoretical stages would be 18 instead of 9. Therefore, in the rectifying section, the number of stages would be 12 and in stripping 6 respectively.

9.3 GVL/furfural vacuum distillation simulation

In this phase of the study, the Aspen Plus software has been used to estimate the purity of the products as top and bottom distillate. However, in the simulation run, the original feed composition of the GVL and furfural has been tested in a certain operating condition such as a number of theoretical plates, reflux and distillate rate. The input and output results are presented below based on the drawn model in Aspen Plus. Here the process simulation carried out in Aspen Plus simulation is given as an example in *Figure 26*.

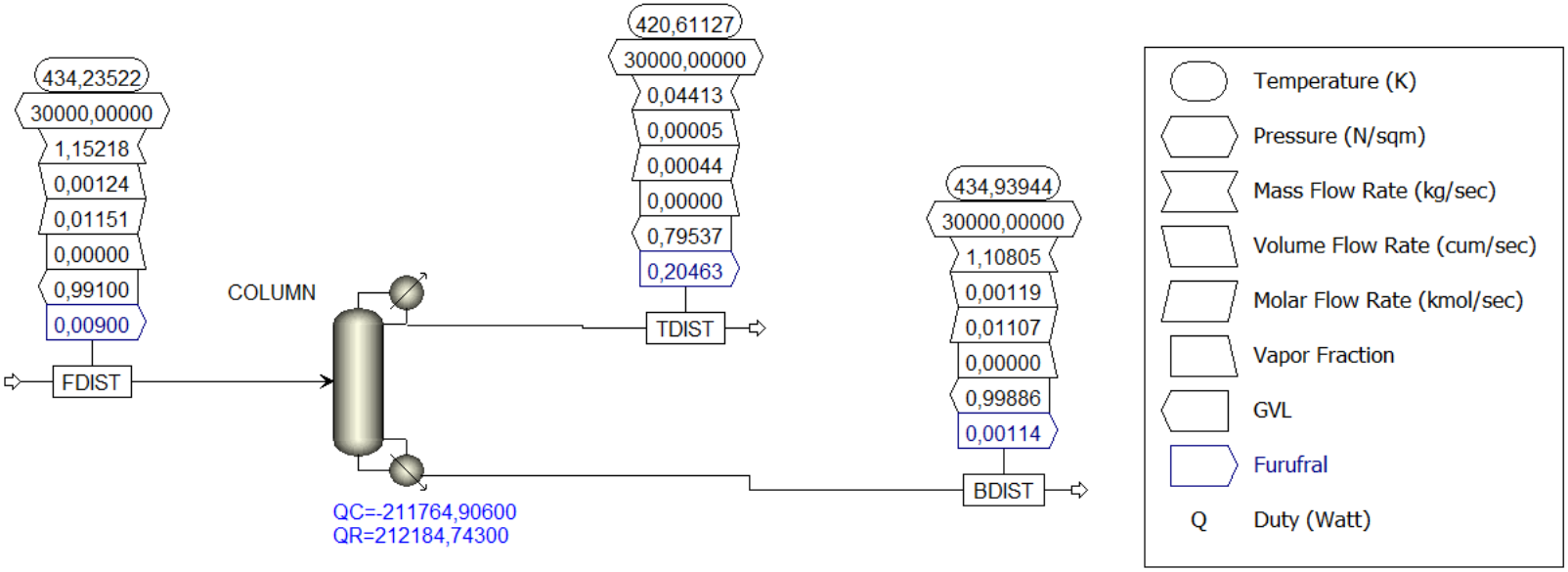

Figure 26. Process simulation illustration for GVL and Furfural distillation using Aspen Plus.

According to *Figure 26*, FDIST represents the feed to the distillation column, where TDIST and BDIST represent the top and bottom products respectively. To carry out the distillation, the input values were given below as below:

Table 6: Input parameters for vacuum distillation of GVL and furfural separation

Input Conditions		**Remarks**
Total No of stages	18	Minimum ×2
Feed stage	12	Above Stage
Reflux ratio	9	Rd, min
Distillate rate	1600	mol/hr
Feed mole fraction, GVL	0.993	-
Feed mole fraction, Furfural	0.007	-
Total feed	41442.5	mol/hr

Simulated results using Aspen Plus software package, based on the above configurations, provides the following stream results *Table 7*:

Table 7: Calculated stream results for vacuum distillation

	BDIST	FDIST	TDIST
Mole Flow, kmol/sec			
GAMMA-01	0.01095	0.01143	0.00048
WATER	0	0	0
FURFU-01	0	0.00008	0.00008
Total Flow, kmol/sec	0.0110	0.0115	0.0006
Total Flow, kg/sec	1.0969	1.1522	0.0553
Total Flow, cum/sec	0.0012	0.0012	0.0001
Temperature, K	435	434	425
Pressure, kPa	30	30	30
Vapor Fraction	0.0000	0.0000	0.0000
Liquid Fraction	1.0000	1.0000	1.0000
Enthalpy, kJ/kmol	-443220	-441600	-409190
Enthalpy, kJ/kg	-4427	-4412	-4110
Enthalpy, Kilowatt	-4856	-5084	-227
Entropy, J/kmol-K	-444	-443	-415
Entropy, J/kg-K	-4.4397	-4.4256	-4.1690
Density, kmol/cum	9.2651	9.2768	9.4960
Density, kg/cum	927.5827	928.5106	945.4829
Average Molecular weight	100.1156	100.0891	99.5670
Liq Vol 60F cum/sec	0.0011	0.0011	0.0001

Total mass balance and the energy balance for the simulated process is given below in *Table 8*.

Table 8: Calculated mass balance and the energy balance for the vacuum distillation

Total	Units	In	Out	Rel. diff
Mole-flow	kmol/hr	41.442	41.442	0
Mass-flow	kg/hr	4147.939	4147.939	-6.34E-14
Enthalpy	kW	-5083.614	-5083.361	-4.98E-05

From above *Table 8*, the relative difference is negligible that, it was considered to be well balanced. In addition to this, the summary of the condenser and the boiler is given in later section 9.4.4.

Based on our findings the top distillate composition and bottom product composition is given in *Table 9* below.

Table 9: Top and bottom product composition of GVL and furfural at the vacuum distillation column

Remarks	Feed		Top		Bottom	
	GVL	Furfural	GVL	Furfural	GVL	Furfural
Mole fraction	0.993	0.007	0.13651	0.86349	0.99957	0.00043

According to the table above indicates that in the top distillate, the furfural considerably pure and contains GVL. Where in the bottom stream GVL seems almost pure as ~100 %. However, to avoid accumulation, it requires to separate furfural pure. Otherwise, it will accumulate in the recycling process. Therefore, different parameters such as different feed compositions, number of theoretical stages, reflux ratio and different flow rate were studied to observe the effect on purity percentage for both components in the top and bottom distillates. Therefore, a sensitivity analysis was carried out, which is presented in the next section below.

9.4 Sensitivity analysis of vacuum distillation for solvent recovery

In this section of study different operating parameters such as feed composition, a number of theoretical plates for vacuum distillation and reflux ratio were studied to estimate furfural recovery. This study provides required data such as feed composition ratio for furfural and GVL in feed stream for optimising operation in a real-life scenario.

9.4.1 Feed composition effects on the purity of Furfural and GVL distillates

In this section, the different mole fraction of furfural in the feed stream was studied. The given parameters such as flow rate, distillate rate and reflux ratio used for different feed composition and the findings are given below.

Table 10 Feed point operating parameters for vacuum distillation of GVL and furfural

Distillate rate, mol/hr	1.6
Flow, mol/hr	44
Reflux	12
No. of plates	18

For above *Table 10*, given parameters were kept constant while the feed composition variability was studied. The calculated mole fraction purity for top and bottom products for different feed composition given below as *Table 23* in Appendix 2. A graph has been plotted to show the feed composition effects on the top and bottom distillates purity at given parameters in *Table 10*. The graphical illustration is given in *Figure 27*.

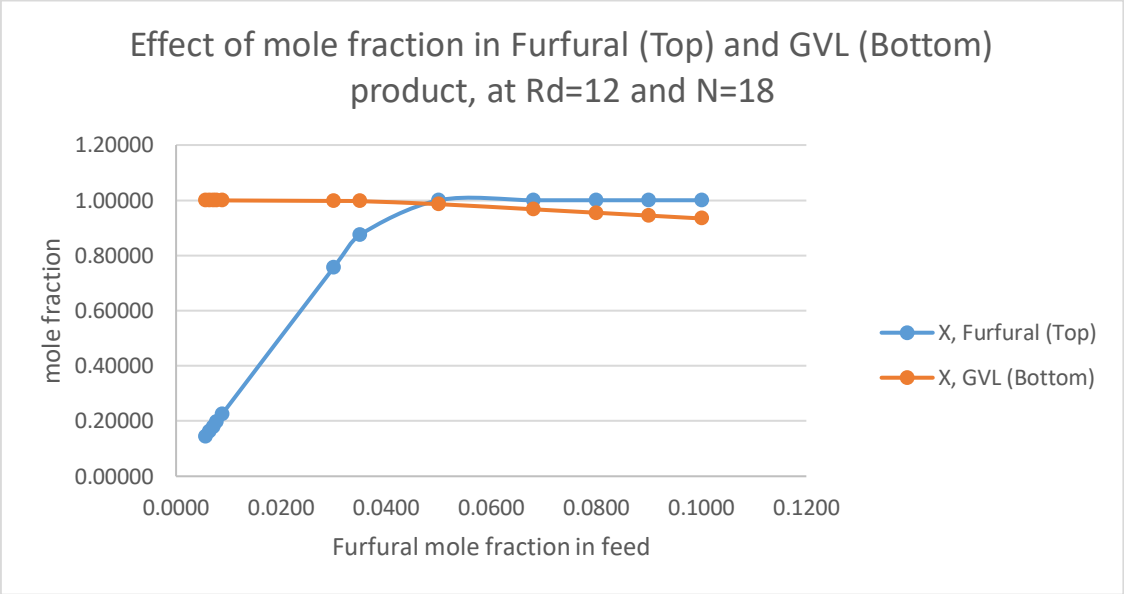

Figure 27. Effect of feed composition on the top and bottom distillate mole fraction

In *Figure 27*, it can be seen that the distillation of furfural gradually improved by increasing the furfural amount in feed composition. In addition, GVL mole fraction in bottom product little decreases while increasing furfural mole fraction at the top of the column. However, the GVL mole fraction in the bottom shows above 0.9334 which is considered to be pure.

9.4.2 Reflux ratio effects on the purity of furfural and GVL as distillates

In this part of the sensitivity analysis, different reflux ratio for different theoretical plates were studied. The defined values from Aspen Plus simulation shows the purity of products as top and bottom distillates as a mole fraction. The calculated results are given in *Table 24* in Appendix 2. The results show an increase of reflux ratio provides higher purity in furfural and GVL mole fraction. A graph was plotted based on the findings and given as *Figure 28*, which shows the purity change with reflux ratio changes.

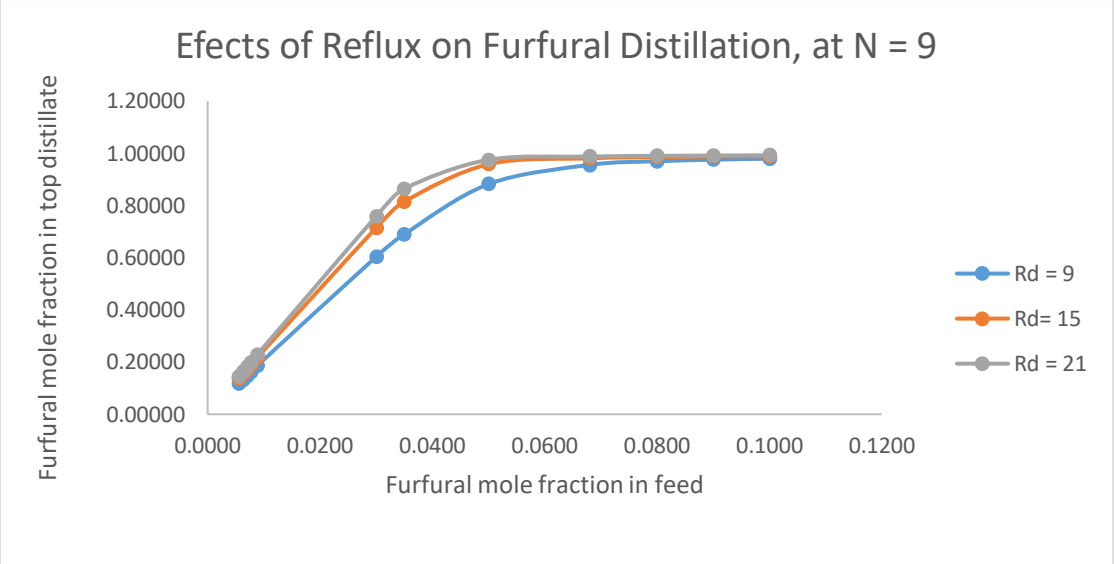

Figure 28. The effect of reflux ratio on the recovery of furfural as top distillate

Figure 28 shows that for the minimum reflux ratio = 9 gives lower furfural recovery as top distillate products than other reflux ratios of 15 and 21 respectively. In addition, the effects of furfural amount in feed composition studied over GVL recovery as bottom distillate for the same number of theoretical stages for different reflux ratio condition. A graph plotted based on the data extracted and tabulated in *Table 24*.

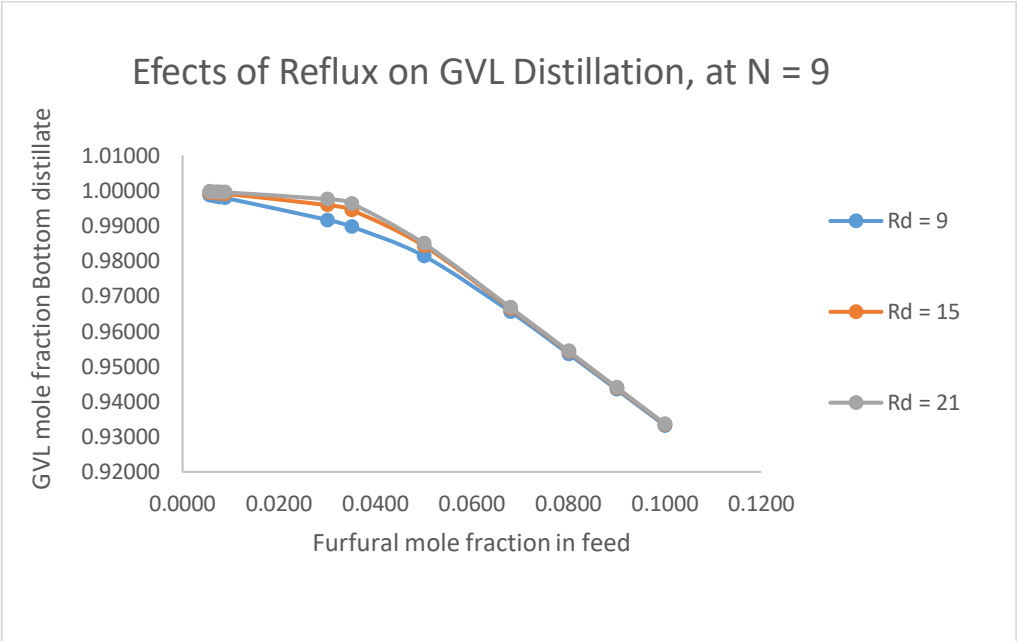

Figure 29. Effect of reflux ratio on GVL recovery as a bottom product for variable feed composition.

From the above *Figure 29*, it can be seen that for the minimum reflux ratio of 9 gives lower GVL mole fraction as bottom distillates. However, the effects of feed composition are predominant compared to the reflux ratio. A similar trend is observed here likely to the previous section where increasing furfural amount in feed composition reduces the mole fraction of GVL in the bottom product. However, the mole fraction of GVL still above 0.9300 which describes it as qualitatively pure. Moreover, in terms of defining optimum values is still seems like the composition (mole fraction) of 0.0500 and 0.9500 for furfural and GVL respectively in feed composition gives relatively higher values of furfural and GVL as top and bottom product.

The effects of a higher number of theoretical stages such as 18, 27 and 36 also studied for reflux ratio values of 9, 15 and 21. Here, the relative graphs are in appendix 1 and results are in appendix 2 given.

From *Figure 37- 42* in Appendix 1, variable theoretical stages and given reflux ratio shows comparably similar trends on the purity of increasing mole fraction of furfural and GVL in top and bottom product respectively same. However, by comparing *Table 25-27* values for different theoretical stages, it can be seen that higher the theoretical stages provides more purity for furfural and GVL. But, the expected purity can be achieved at higher furfural composition.

Observation indicates that feed composition has significant effects on the purity of top and bottom distillates over other parameters changes.

9.4.3 No. of theoretical stages effects on the purity of Furfural and GVL distillates

To summarise the whole scenario in a more simple way, there is three feed composition chosen based on the above findings above, to show relatability of feed composition, number of theoretical stages and reflux ration. Here below, the Table is presented for total feed flow of 44000 mol/hr and distillate rate of 1600 mol/hr. Simulation matrix for this study is given below as *Table 11*.

Table 11: Effect of theoretical stages on distillates composition with variable feed composition and reflux ratio

No. of plates	Inlet		Furfural mole fraction, Top			GVL mole fraction, Bottom		
	Feed composition, mole fraction		Reflux Ratio, Rd			Reflux Ratio, Rd		
	Furfural	GVL	9	15	21	9	15	21
9	0.0070	0.9930	0.14801	0.17250	0.18151	0.99832	0.99925	0.99958
18	0.0070	0.9930	0.16470	0.18629	0.19049	0.99895	0.99977	0.99992
27	0.0070	0.9930	0.17232	0.19035	0.19209	0.99924	0.99992	0.99999
36	0.0070	0.9930	0.17684	0.19174	0.19242	0.99941	0.99997	1.00000
9	0.0500	0.9500	0.88254	0.95874	0.97565	0.98142	0.98429	0.98493
18	0.0500	0.9500	0.99974	0.99998	0.99999	0.98584	0.98585	0.98585
27	0.0500	0.9500	1.00000	1.00000	1.00000	0.98585	0.98585	0.98585
36	0.0500	0.9500	1.00000	1.00000	1.00000	0.98585	0.98585	0.98585
9	0.0900	0.9100	0.97605	0.98811	0.99199	0.94344	0.94389	0.94404
18	0.0900	0.9100	0.99997	0.99999	0.99999	0.94434	0.94434	0.94434
27	0.0900	0.9100	1.00000	1.00000	1.00000	0.94434	0.94434	0.94434
36	0.0900	0.9100	1.00000	1.00000	1.00000	0.94443	0.94434	0.94434

A graph *Figure 30* has now been plotted to visualize the furfural distillates mole fraction as a function of different stages, reflux ratio and feed composition.

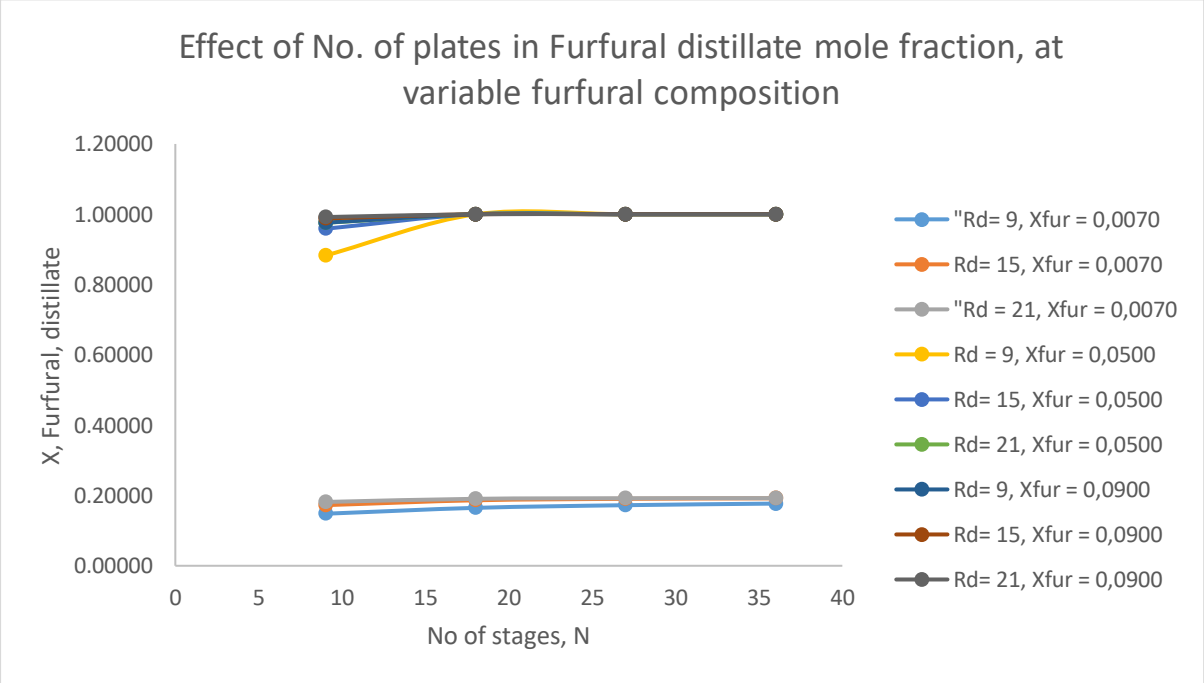

Figure 30. Effect of No. of plates in furfural distillate mole fraction, at variable furfural composition

As, furfural distillation shows higher purity with a feed composition of furfural and GVL 0.0500 and 0.9500 or above respectively. However, with the minimum reflux ratio, the purity is always less. The same trend can be seen for GVL distillates at the bottom too. However, GVL purity reduces with increasing furfural amount in the feed as we have seen earlier.

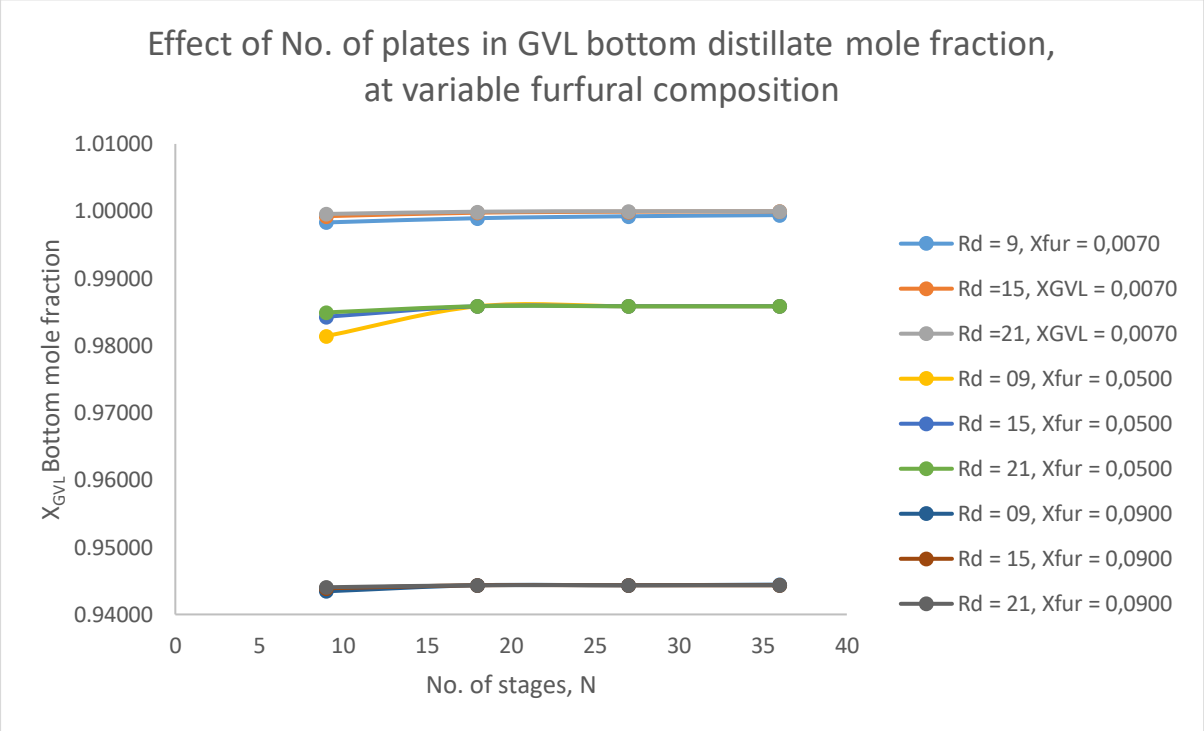

Figure 31. Effect of No. of plates in GVL bottom product mole fraction, at variable furfural composition

9.4.4 No. of theoretical stages effects on condenser and reboiler heat duty

In this section of this chapter, it is represented the condenser heat duty Q_C and reboiler heat duty, Q_R values which were generated by the simulation process. Where Q_C denotes heat duty for condenser and Q_R denotes heat duty for reboiler. *Table 12* below only represents selected heat duty values for selected furfural feed composition.

Table 12 Heat duty results for condenser and reboiler for vacuum distillation at different operating condition

No. of plates	Inlet		Q_C			Q_R		
	Feed composition, mole fraction		Reflux Ratio, Rd			Reflux Ratio, Rd		
	Furfural	GVL	9	15	21	9	15	21
9	0.0070	0.9930	-211041.4	-338265.0	-465354.4	211274.2	338576.6	465697.8
18	0.0070	0.9930	-211300.3	-338530.3	-465599.5	211586.4	338890.8	465974.6
27	0.0070	0.9930	-211413.0	-338615.3	-465621.2	211723.9	338989.8	466002.9
36	0.0070	0.9930	-211466.7	-338639.8	-465645.9	211793.8	339019.5	466028.0
9	0.0500	0.9500	-200159.1	-315720.4	-432660.2	204034.9	320135.3	437196.3
18	0.0500	0.9500	-195684.8	-313080.1	-430484.0	200396.4	317793.5	435194.6
27	0.0500	0.9500	-195674.2	-313078.7	-430483.2	200387.7	317789.4	435196.8
36	0.0500	0.9500	-195674.2	-313078.7	-430483.2	200387.8	317789.4	435193.9
9	0.0900	0.9100	-196639.7	-313850.3	-431206.2	200336.2	317622.1	435010.0
18	0.0900	0.9100	-195675.3	-313079.3	-430483.7	199529.5	316933.6	434338.0
27	0.0900	0.9100	-195674.2	-313078.7	-430483.2	199520.7	316925.3	434337.6
36	0.0900	0.9100	-195674.2	-313078.7	-430483.2	199528.5	316925.3	434329.8

In terms of above-calculated results using Aspen Plus simulation software, heat duty changes using different feed composition of furfural and at different reflux ratio has been plotted.

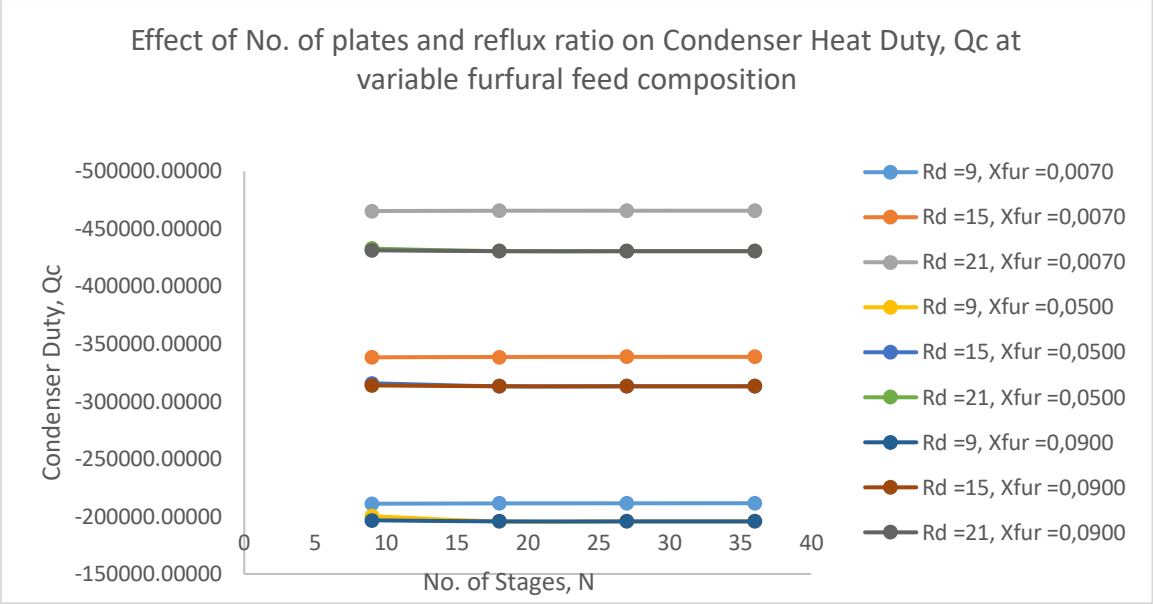

Figure 32. Effect of No. of plates and reflux ratio on condenser Heat Duty, Q_c at variable furfural feed composition

According to *Figure 32* above, it can be seen that the furfural amount in feed composition has a significant effect on the required heat duty on the condenser. However, the effect of reflux ratio is very significant and makes it obvious. The effect of theoretical stages is negligible compared to other parameters. But, a higher number of theoretical stages will add initial installation costs.

Reboiler heat duty, Q_R also plotted following similar parameter conditions.

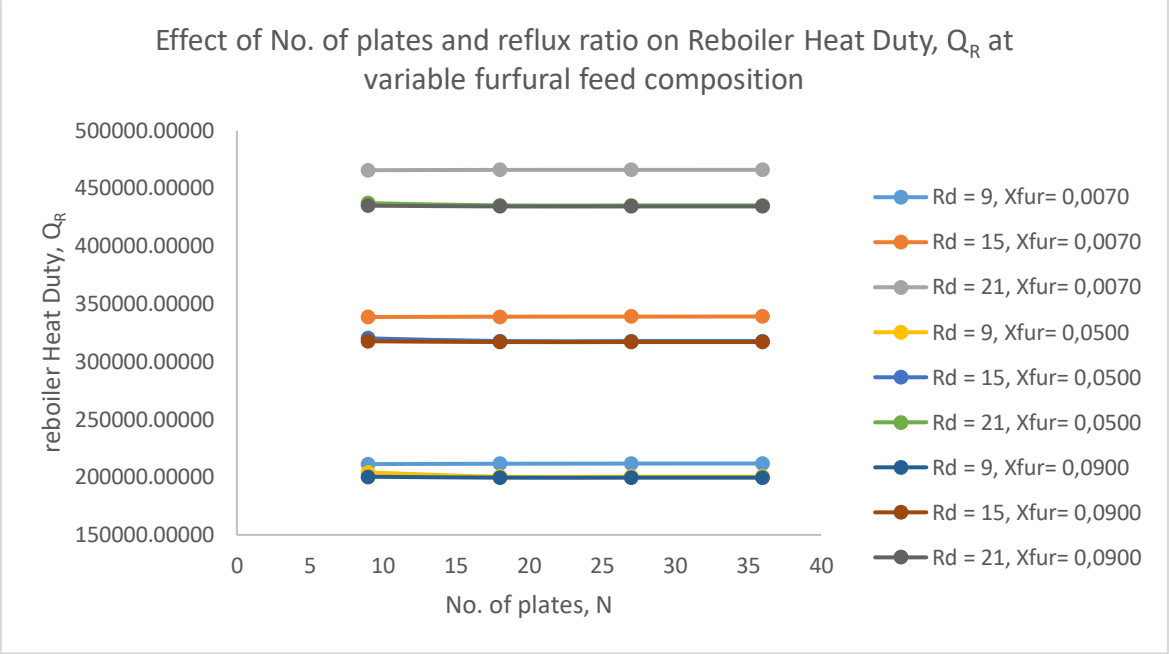

Figure 33. Effect of No. of plates and reflux ratio on reboiler Heat Duty, Q_R at variable furfural feed composition

Figure 33, above shows also a similar trend likely to the condenser heat duty is opposite.

9.5 GVL/furfural vacuum distillation using stripping column

In this section of the study, considered with hypotheses that majority of GVL can be removed using the stripping column before the vacuum distillation process starts. Establishment of the strippers prior to the vacuum distillation column will allow the process to be less energy intensive as less amount of evaporation will be carried out.

Here below a model summary is given below *Table 13*

Table 13: Model summary of vacuum distillation enabling strippers.

Name	DIST1	STRIPPE1	STRIPPE2
Property method	UNIF-DMD	UNIF-DMD	UNIF-DMD
Use true species approach for electrolytes	YES	YES	YES
Free-water phase properties method	STEAM-TA	STEAM-TA	STEAM-TA
Water solubility method	3	3	3
Number of stages	30	20	20
Condenser	TOTAL	NONE	NONE
Reboiler	KETTLE	KETTLE	KETTLE
Number of phases	2	2	2
Free-water	NO	NO	NO
Top stage pressure [kPa]	30	30	30
Specified reflux ratio	5		
Specified bottoms rate [kmol/sec]		0.00777778	0.0025
Specified distillate rate [mol/hr]	370		
Calculated molar reflux ratio	5	3	3
Calculated bottoms rate [kmol/sec]	0.0011	0.0078	0.0025
Calculated boilup rate [kmol/sec]	0.0006	0.0038	0.0013
Calculated distillate rate [kmol/sec]	0.0001	0.0037	0.0012
Condenser / top stage temperature [K]	395.1230	434.3570	432.9360
Condenser / top stage pressure [kPa]	30	30	30
Condenser / top stage heat duty [Watt]	-27205.10	0.00	0.00
Condenser / top stage reflux rate [kmol/sec]	0.00	0.01	0.00
Reboiler pressure [kPa]	30	30	30
Reboiler temperature [K]	434.97	435.04	435.03
Reboiler heat duty [Watt]	28228.63	174525.04	58338.18

Also, another model summary of heaters added in the simulation flowsheet is given below.

Table 14: Model summary of heaters added to stripping columns

Name	STRI1CON	STRI2CON
Property method	UNIF-DMD	UNIF-DMD
Use true species approach for electrolytes	YES	YES
Free-water phase properties method	STEAM-TA	STEAM-TA
Water solubility method	3	3
Specified pressure [kPa]	30	30
Calculated pressure [kPa]	30	30
Calculated temperature [K]	432.63	428.28
Calculated vapor fraction	0.00	0.00
Calculated heat duty [Watt]	-174467.00	-58184.65
Net duty [Watt]	-174467.01	-58184.65

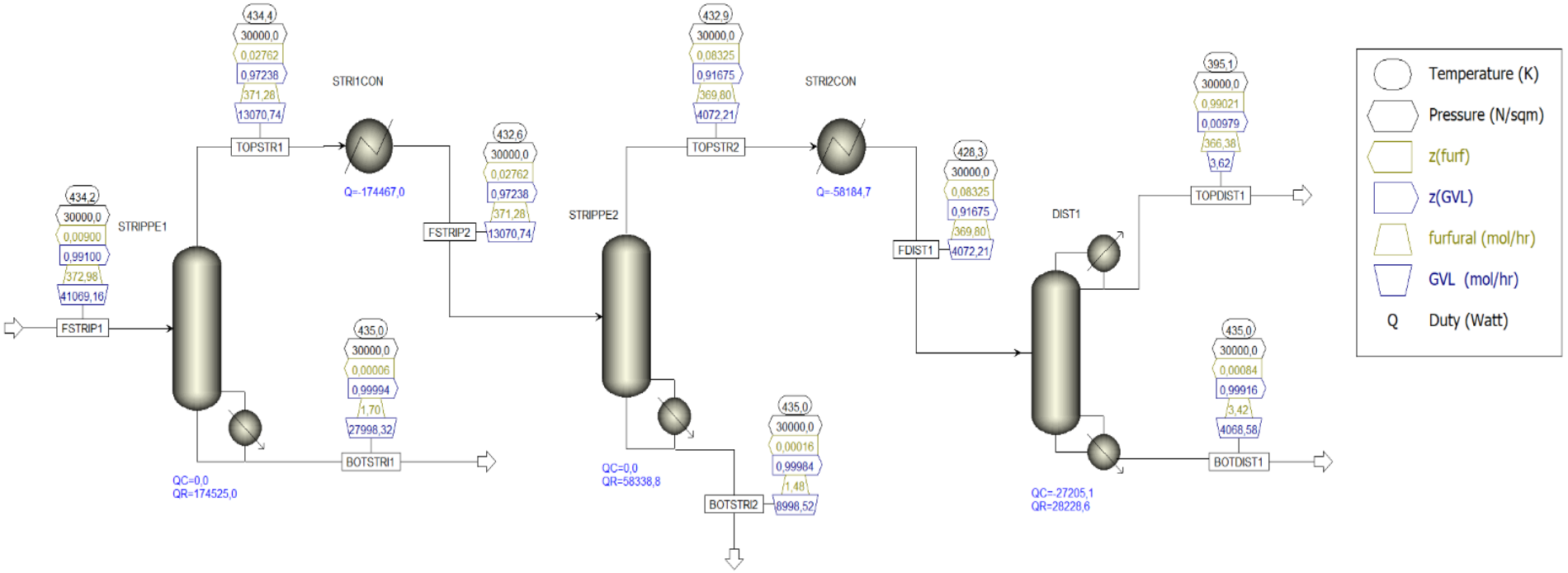

Figure 34. Aspen Plus simulation of GVL and furfural vacuum distillation using stripping columns with a distillation column

Applying the UNIF-DMD (UNIFAC-Dortmund) method for the simulation gives the stream results below as *Table 15*

Table 15: Results summary of GVL/furfural vacuum distillation using stripping column results

	Units	FSTRIP1	TOPSTR1	BOTSTRI1	FSTRIP2	TOPSTR2	BOTSTRI2	FDIST1	TOPDIST1	BOTDIST1
From			STRIPPE1	STRIPPE1	STRI1CON	STRIPPE2	STRIPPE2	STRI2CON	DIST1	DIST1
To		STRIPPE1	STRI1CON		STRIPPE2	STRI2CON		DIST1		
Phase:		Liquid	Vapor	Liquid	Liquid	Vapor	Liquid	Liquid	Liquid	Liquid
Component Mole Flow										
Fufural	kmol/hr	0.373	0.371	0.002	0.371	0.370	0.001	0.370	0.366	0.003
GVL	kmol/hr	41.069	13.071	27.998	13.071	4.072	8.999	4.072	0.362	4.069
Component Mole Fraction										
Furfural		0.00900	0.02762	0.00006	0.02762	0.08325	0.00016	0.08325	0.99021	0.00084
GVL		0.99100	0.97238	0.99994	0.97238	0.91675	0.99984	0.91675	0.00979	0.99916
Mole Flow	kmol/hr	41.44	13.44	28.00	13.44	4.44	9.00	4.44	0.37	4.07
Mass Flow	kg/hr	4147.56	1344.28	2803.28	1344.28	443.23	901.05	443.23	35.57	4.08
Volume Flow	CUM/sec	0.00	0.44	0.00	0.00	0.15	0.00	0.00	0.00	0.00
Temperature	K	434.24	434.36	435.04	432.63	432.93	435.03	428.28	395.12	434.97
Pressure	Mpa	0.03	0.03	0.03	0.03	0.03	0.03	0.03	0.03	0.03
Vapour Fraction		0.00	1.00	0.00	0.00	1.00	0.00	0.00	0.00	0.00
Liquid Fraction		1.00	0.00	1.00	1.00	0.00	1.00	1.00	1.00	1.00
Solid Fraction		0.00	0.00	0.00	0.00	0.00	0.00	0.00	0.00	0.00
Molar Enthalpy	kJ/kmol	-441110.00	-389770.00	-443310.00	-436490.00	-375450.00	-443290.00	-422610.00	-186900.00	-443120.00
Mass Enthalpy	kJ/kg	-4407.49	-3897.46	-4427.94	-4364.69	-3762.74	-4427.71	-4235.33	-1944.33	-4426.16
Enthalpy Flow	KW	-5077.87	-1455.36	-3447.99	-1629.82	-463.27	-1108.22	-521.45	-19.21	-501.22
Molar Entropy	kJ/kmol-K	-442.51	-330.71	-444.58	-438.41	-317.15	-444.55	-426.47	-233.71	-444.38
Mass Entropy	kJ/kg-K	-4.42	-3.31	-4.44	-4.38	-3.18	-4.44	-4.27	-2.43	-4.44
Molar Density	kmol/CUM	9.28	0.01	9.26	9.31	0.01	9.26	9.41	10.92	9.27
Mass Density	kg/CUM	928.79	0.84	927.53	931.37	0.84	927.54	938.76	1049.70	927.64
Average Molecular Weight		100.08	100.01	100.12	100.01	99.78	100.12	99.78	96.13	100.11

10. Simulation of compressor

In this section, it was more focused on using a compressor to compress the CO_2 flow comes from the liquid extraction phase where CO_2 gets compressed and reduced temperature before recycling into the system. In property set up during Aspen simulation, it was used REFPROP methods assuming pure fluid properties with no parameter's estimation. In the compressor block of the flowsheet, it was used isentropic compressor model with fixed discharge pressure of 7.5 MPa in the output stage where it was maintained equal pressure ratio. Here below, the 3-stage compression and each stage outlet temperature is given as *Table 16*

Table 16. Three-stage compression outlet temperature

Stage	1	2	3
Specification	Outlet Temp, K	Outlet Temp, K	Outlet Temp, K
Value	310	305	298.15

The flow chart in Aspen plus software is given below. Three-stage compression is embedded within the block COMP in *Figure 35*.

The model summary is given below as *Table 17*.

Table 17 Aspen plus simulation model summary of CO_2 compression

Name	COMP
Property method	REFPROP
Use true species approach for electrolytes	YES
Free-water phase properties method	STEAM-TA
Water solubility method	3
Number of stages	3
Fix discharge pressure from last stage [MPa]	7.5

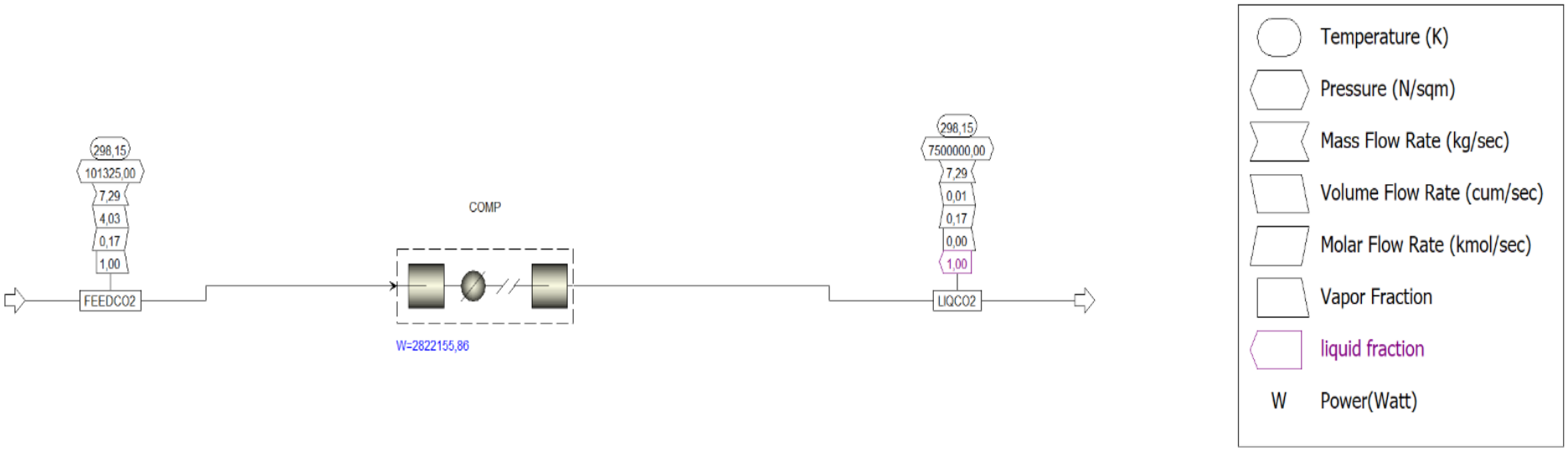

Figure 35 Aspen Plus simulation of multi-stage CO_2 compression

Here below the Aspen Plus simulated result summary of different streams are given.

Table 18 Compression result summary of CO_2

	Units	FEEDCO2	LIQCO2
From			COMP
To		COMP	
Phase:		Vapor	Liquid
Component Mole Flow			
CO2	kmol/hr	596.68	596.68
Mole Flow	kmol/hr	596.68	596.68
Mass Flow	kg/hr	26259.85	26259.85
Volume Flow	CUM/hr	14524.50	34.47
Temperature	K	298.15	298.15
Pressure	MPa	0.101325	7.50
Vapour Fraction		1.00	0.00
Liquid Fraction		0.00	1.00
Solid Fraction		0.00	0.00
Molar Enthalpy	kJ/mol	-393.55	-404.12
Mass Enthalpy	kJ/kg	-8942.36	-9182.60
Enthalpy Flow	KW	-65229.16	-66981,57
Molar Entropy	kJ/kmol-K	2787845.00	-64281.37
Mass Entropy	kJ/kg-K	0.063	-1.461
Molar Density	kmol/CUM	0.041	17.311
Mass Density	kg/CUM	1.81	761.87
Average Molecular Weight		44.01	44.01

Total cooling duty for compression and temperature reduction values calculated results are given below *Table 19*

Table 19 Simulated results summary of cooling heat duty

Number of stages	3
Fix discharge pressure from last stage [MPa]	7.5
Outlet pressure [MPa]	7.5
Total work [kW]	2822.16
Total cooling duty [kW]	-4574.57
Net work required [kW]	2822.16
Net cooling duty [kW]	-4574.57

11. Simulation of Liquid-Liquid extraction

In this section, it was carried out the liquid-liquid extraction using CO_2 as a liquid. However, the process was carried out making an assumption that only the main components water, GVL and CO_2 are entering into the feed stream. Furfural was not take in count due to its small quantity compared to other main components for process simplicity. In this simulation flow sheet, the decanter unit model was used as it was mentioned in an earlier section of 8.2. In the property method, it was used KLL correlation and as the main component, it was assumed that the feed flow contains mostly GVL and water. The feed of furfural was ignored as the furfural amount in the composition is tiny in amount. The addition of liquid CO_2 fluid from another end of the decanter. The process was carried out in 3 stages. There was no sensitivity analysis was carried out like vacuum distillation. The liquid extraction result summary and balance data can be found in Appendix 3 in *Table 28*. The process simulation flow sheet can be seen below as *Figure 36*. In the feed composition, it was only GVL and water entered to stage 1 (STAGE1). Liquid CO_2 flow was given into stage 3 using (CO2SOLV) stream. However, during simulation input, it was entered a scale-up amount of mass flow but with the similar mole fraction of GVL and water data which can be seen from *Figure 5*. However, after running the heat duty for each stages data has been calculated using Aspen simulation software. Those data are given below.

Table 20: Heat duty data for liquid extraction using liquid CO_2

Name	STAGE1	STAGE2	STAGE3
Pressure [MPa]	7.50	7.50	7.50
Temperature [K]	298.15	298.15	298.15
Outlet temperature [K]	298.15	298.15	298.15
Outlet pressure [MPa]	7.50	7.50	7.50
Calculated heat duty [Watt]	-40954.80	-5205.40	-606.00
Net duty [Watt]	-40954.80	-5205.40	-606.00

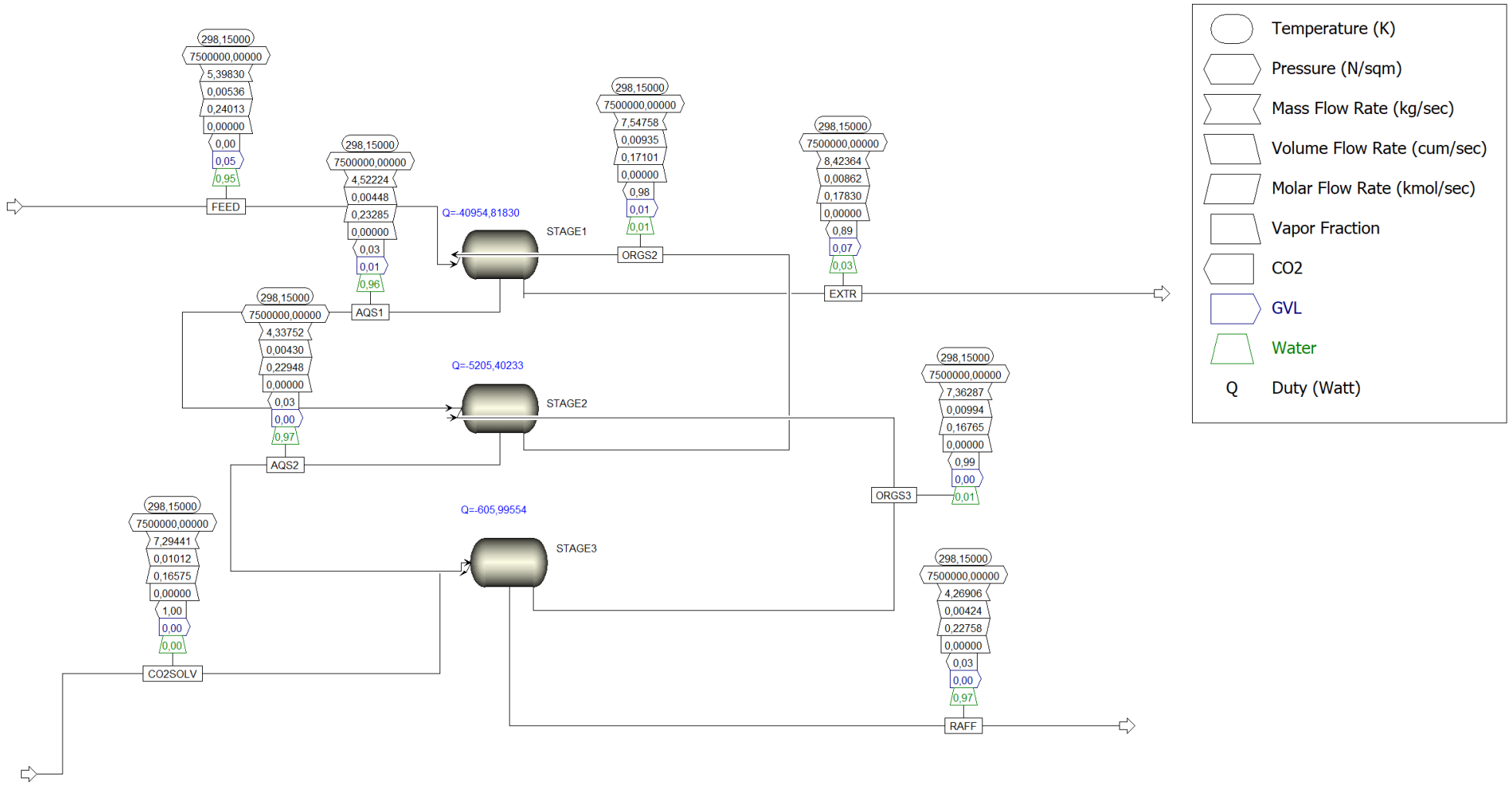

Figure 36 Process simulation flowsheet of liquid-liquid extraction using liquid CO_2

In addition, RAFF describes the raffinate stream, EXTR describes the extract contains mostly GVL and CO_2. Also, AQS1, AQS2 describes the aqueous phase and ORGS2, ORGS3 stream contains organics layer.

12. Energy Calculation

Here below, it was tabulated the energy consumption for GVL recovery from spent liquor based on the total GVL entered in liquid-liquid extraction feed stream. From Figure 5, in laboratory-scale GVL in spent liquor amount is 47.07g. By assuming the scale-up of the process at 10000 times gives the feed mass flow rate of 4707.00 $kghr^{-1}$ which equivalents to 1.308 kgs^{-1}. Therefore, the mass flow rate was taken in count in the entire simulation process. However, other energy consumption sources such as pumps and so on have not been taken in count in this study. The energy consumption for GVL recovery is expressed as $kJkg^{-1}$ and given in *Table 21*. So, the overall GVL recovery process requires 6088.52 $kJkg^{-1}$ GVL in the feed.

Table 21 Energy consumption of GVL recovery process at different units

	Vacuum Distillation					**Compressor**	**Liquid-Liquid extraction**		
	Stripper 1	Stripper 2	Distillation column	Heater 1	Heater 2		Stage 1	Stage 2	Stage 3
Condenser heat duty, Qc, kW	0	0	27.21	0	0	4574.57	0	0	0
Reboiler heat duty, Qr, kW	174.53	58.34	28.23	0	0	0	0	0	0
Heat duty, Q, kW	0	0	0	174.467	58.185	0	37.643	4.851	0.57
Total work, W, kW	0	0	0	0	0	2822.16	0	0	0
Total, kW	174.53	58.34	55.43	174.47	58.19	7396.72	37.64	4.85	0.57
Energy requirements, kJ/kg GVL in feed	133.48	44.62	42.40	133.44	44.50	5657.15	28.79	3.71	0.44

13. Results & Discussion

In this study, all different steps were studied individually instead of under a uniform model. This study was conducted for a preliminary understanding of energy consumption for GVL recovery from the spent liquors. In liquid extraction stage using liquid CO_2, it was aimed mainly to separate the water from GVL. In the compressor section, it was targeted to compress the CO_2 at room temperature and pressurize it at 7.5 MPa. Vacuum distillation separately studied to separate furfural and GVL to avoid the accumulation of furfural in GVL recycling.

According to vacuum distillation sensitivity study and process simulation, it was found that the almost pure recovery of GVL and furfural is possible. However, feed composition plays a significant role in terms of achieving target mole or mass fraction of top and bottom products. Also, the higher the reflux ratio and a high number of the theoretical stage for separation gives higher the purity percentage, despite the high operation costs. Therefore, optimum feed composition is required to find to operate the process, which therefore showed in the sensitivity analysis of vacuum distillation that, the feed composition (mole fraction) of 0.0500 and 0.9500 for furfural and GVL respectively in feed composition gives relatively higher values of furfural and GVL as top and bottom product in out-stream. Lower feed composition of furfural (mole fraction) than this might make the separation process relatively difficult.

There were two case studies on vacuum distillation carried out. In one case study, it was determined the energy consumption and purity of GVL and furfural using only distillation columns. Another case study was based on the addition of stripping columns before the distillation column. Above findings, shows that enabling stripping columns before the distillation columns help to improve the separation of GVL and furfural. Addition of two stripping columns removes most of the GVL and reduce the amount of GVL in the distillation column. Therefore, in terms of estimating the energy consumption for distillation, vacuum distillation with stripping columns simulation was taken in count.

In terms of CO_2 compression, as inlet feed to the compressor, it was assumed to be the same amount CO_2 entered into the liquid-liquid extraction column. After 3 stages of compression, it possible to deliver fix discharge pressure of 7.5 MPa and room temperature of 298K. However, it was assumed that water was fully removed during liquid-liquid extraction. Therefore, only CO_2 was taken in the count during the compression simulation.

In liquid-liquid extraction, the idea was to remove the aqueous solution as much as possible. Therefore, enabling three decanters in the simulation process carried out to remove the aqueous phase from the feed stream.

The calculated results show that the compressor is the highly intensive unit in the process consumes approximately ≈92% of the total energy. In addition, the strippers and heaters are the following energy-intensive units. Liquid-liquid extraction column is the less energy required stage. However, in terms of feeding solution into the liquid-liquid extraction column, it would require considering the pump energy requirement.

14. Future study outlook

In this study, it was studied only the main component which are high in an amount in spent liquor. However, more complex systems such as additional components behaviour can be studied for a better understanding of process behaviour and its feasibility. Also, in terms of energy consumption, pump work and other possible heat-exchangers can be taken in count for determining optimized energy consumption values. Finally, a uniform simulation process might require describing the whole process better.

References

Advantages of Using Cubic Equations of State; Phase Relations in Reservoir Engineering. Available: https://www.e-education.psu.edu/png520/m11_p5.html [02.02.2019].

Yaws' Critical Property Data for Chemical Engineers and Chemists
Copyright © 2012; 2013; 2014 Knovel.

AASEN, A., HAMMER, M., SKAUGEN, G., JAKOBSEN, J.P. and WILHELMSEN, Ø, 2017. Thermodynamic models to accurately describe the PVTxy-behavior of water / carbon dioxide mixtures. Fluid Phase Equilibria, **442**, pp. 125-139.

ANASTAS, P.T. and WARNER, J.C., 2000. Green chemistry: theory and practice. Oxford university press.

ANONYMOUS, a. Aspen Physical Property System-Physical Property Methods and Models 11.1. Cambridge, MA.: Aspen Technology, Inc.

ANONYMOUS, b. Supporting Information for Liquid-liquid extraction for recovering low margin chemicals: Thinking beyond the partition ratio.

ASPEN TECHNOLOGY, I., a. Aspen Plus STEADY STATE SIMULATION; User Models V.10.1 -Reference Manuals.

ASPEN TECHNOLOGY, I., b. Methods for Calculating the liquid-liquid distribution coefficients (KLL).

BERK, Z., 2013. Chapter 11 - Extraction. San Diego: Academic Press.

DESIGN INSTITUTE FOR PHYSICAL PROPERTIES, SPONSORED, BY AICHE, a. CARBON DIOXIDE- Temperature-Independent Properties; DIPPR Project 801 - Full Version. Design Institute for Physical Property Research/AIChE.

DESIGN INSTITUTE FOR PHYSICAL PROPERTIES, SPONSORED, BY AICHE, b. FURFURAL- FURFURAL; DIPPR Project 801 - Full Version. Design Institute for Physical Property Research/AIChE.

DESIGN INSTITUTE FOR PHYSICAL PROPERTIES, SPONSORED, BY AICHE, c. WATER- Temperature-Independent Properties; DIPPR Project 801 - Full Version. Design Institute for Physical Property Research/AIChE.

ELLIOTT, J. RICHARD, LIRA, CARL T., 2012. Introductory chemical engineering thermodynamics.

FANG, W. and SIXTA, H., 2015. Advanced Biorefinery based on the Fractionation of Biomass in γ-Valerolactone and Water. ChemSusChem, **8**(1), pp. 73-76.

FEGYVERNEKI, D., ORHA, L., LÁNG, G. and HORVÁTH, I.T., 2010. Gamma-valerolactone-based solvents. Tetrahedron, **66**(5), pp. 1078-1081.

FELE, L. and GRILC, V., 2003. Separation of furfural from ternary mixtures. Journal of Chemical & Engineering Data, **48**(3), pp. 564-570.

FREDENSLUND, A., JONES, R.L. and PRAUSNITZ, J.M., 1975. Group-contribution estimation of activity coefficients in nonideal liquid mixtures. AIChE Journal, **21**(6), pp. 1086-1099.

GAUBE, J., 1982a. J. Gmehling, U. Onken, W. Arlt: Vapor-Liquid-Equilibrium Data Collection, in der Reihe: Chemistry Data Series, Vol. I. Parts 3 + 4 Aldehydes and Ketones Ethers, Dechema, Frankfurt 1979. 624 Seiten. Part 6a Aliphatic Hydrocarbons C4-C6, Dechema, Frankfurt 1980, 687 Seiten. Part 6b Aliphatic Hydrocarbons C7 – C18, Dechema, Frankfurt 1980, 506 Seiten. Part 7 Aromatic Hydrocarbons, Dechema, Frankfurt 1980, 563 Seiten. Part 2c Organic Hydroxy Compounds: Alcohols (Supplement 1), Dechema, Frankfurt 1982, 696 Seiten. Part 1a Aqueous-Organic Systems (Supplement 1), Dechema, Frankfurt 1982, 715 Seiten. Berichte der Bunsengesellschaft für physikalische Chemie, **86**(11), pp. 1087-1088.

GAUBE, J., 1982b. J. M. Sørensen, W. Arlt: Liquid-Liquid Equilibrium Data Collection, in der Reihe: Dechema Chemistry Data Series, Vol. V., Part 1: Binary Systems. 622 Seiten, Preis: DM 156,-; Part 2: Ternary Systems. 625 Seiten, Preis DM 176,-; Part 3: Ternary and Quaternary Systems. 604 Seiten, Preis: DM 173,-; DECHEMA, Frankfurt, 1979, 1980, 1980. Berichte der Bunsengesellschaft für physikalische Chemie, **86**(8), pp. 761.

GHASEMIAN, N., KALBASI, M. and PAZUKI, G., 2013. Experimental Study and Mathematical Modeling of Solubility of CO2 in Water: Application of Artificial Neural Network and Genetic Algorithm. Journal of Dispersion Science and Technology, **34**(3), pp. 347-355.

GMEHLING, J., LOHMANN, J., JAKOB, A., LI, J. and JOH, R., 1998. A Modified UNIFAC (Dortmund) Model. 3. Revision and Extension. Industrial & Engineering Chemistry Research, **37**(12), pp. 4876-4882.

HAAR, L., GALLAGHER, J.S. and KELL, G.S., 1984. NBS/NRC Steam Tables. Thermodynamic and Transport Properties and Computer Programs for Vapor and Liquid States of Water in SI Units. Hemisphere Publishing Corporation, Washington.

HAVASI, D., MIZSEY, P. and MIKA, L.T., 2016. Vapor–Liquid Equilibrium Study of the Gamma-Valerolactone–Water Binary System. Journal of Chemical & Engineering Data, **61**(4), pp. 1502-1508.

HYATT, J.A., 1984. Liquid and supercritical carbon dioxide as organic solvents. The Journal of organic chemistry, **49**(26), pp. 5097-5101.

KERTON, F.M. and MARRIOTT, R., 2013. Alternative solvents for green chemistry. Royal Society of chemistry.

KHOURY, F.M., 2014. Multistage Separation Processes. 4th edn. CRC Press.

LAW, J.D. and TODD, T.A., 1.12.2008. Liquid-Liquid Extraction Equipment, Introduction to Nuclear Chemistry and Fuel Cycle Separations,NAshville, TN,12/16/2008,12/18/2008 1.12.2008, Idaho National Laboratory (INL).

LE, H.Q., MA, Y., BORREGA, M. and SIXTA, H., 2016. Wood biorefinery based on gamma]-valerolactone/water fractionation. Green Chemistry, **18**(20), pp. 5466-5476.

LÊ, H.Q., POKKI, J., BORREGA, M., UUSI-KYYNY, P., ALOPAEUS, V. and SIXTA, H., 2018. Chemical Recovery of γ-Valerolactone/Water Biorefinery. Industrial & Engineering Chemistry Research, **57**(44), pp. 15147-15158.

LE, H., POKKI, J., MA, Y., BORREGA, M., ALOPAEUS, V. and SIXTA, H., 2017. γ-valerolactone-based biorefinery: a shortcut from wood to textile fibers, Cellulose Materials Doctoral Students Conference, 23 Oct 2017 → 25 Oct 2017 2017.

LEONARD, R.H., 1956. Levulinic Acid as a Basic Chemical Raw Material 1331. Ind. Eng. Chem, **48**.

LESTARI, G., SALARI, A., ABOLHASANI, M. and KUMACHEVA, E., 2016. A microfluidic study of liquid–liquid extraction mediated by carbon dioxide. Lab Chip, **16**(14), pp. 2710-2718.

LI, X., JIA, P. and WANG, T., 2016. Furfural: a promising platform compound for sustainable production of C4 and C5 chemicals. ACS Catalysis, **6**(11), pp. 7621-7640.

LOHMANN, J., JOH, R. and GMEHLING, J., 2001. From UNIFAC to Modified UNIFAC (Dortmund). Industrial & Engineering Chemistry Research, **40**(3), pp. 957-964.

MÄNNISTÖ, M., POKKI, J. and ALOPAEUS, V., 2018. Phase equilibria of aqueous bio-component mixtures with different solvents for the design of a liquid-liquid extraction unit, Aalto University.

MATSOUKAS, T., 2013. Fundamentals of Chemical Engineering Thermodynamics: With Applications to Chemical Processes. Prentice Hall.

MATTHEWS, J.B., SUMNER, J.F. and MOELWYN-HUGHES, E.A., 1950. The Vapor Pressures of Certain Liquids 797. Trans. Faraday Soc., **46**.

MCCABE, W.L. and THIELE, E.W., 1925. Graphical Design of Fractionating Columns. Industrial & Engineering Chemistry, **17**(6), pp. 605-611.

MCCOY, S.T. and RUBIN, E.S., 2008. An engineering-economic model of pipeline transport of CO2 with application to carbon capture and storage.

MCHUGH, M. and KRUKONIS, V., 2013. Supercritical fluid extraction: principles and practice. Elsevier.

NALAWADE, S.P., PICCHIONI, F. and JANSSEN, L., 2006. Supercritical carbon dioxide as a green solvent for processing polymer melts: processing aspects and applications. Progress in polymer science, **31**(1), pp. 19-43.

PHELPS, C.L., SMART, N.G. and WAI, C.M., 1996. Past, Present, and Possible Future Applications of Supercritical Fluid Extraction Technology. Journal of chemical education, **73**(12), pp. 1163.

POKKI, J., 2017. Engineering Thermodynamics,
Separation Processes, part 1, CHEM-E7100, Lecture 5: Liquid-liquid extraction. Aalto University, Department of Chemical and Metallurgical Engineering: .

POKORNÝ, V., ŠTEJFA, V., FULEM, M., ČERVINKA, C. and RŮŽIČKA, K., 2017. Vapor Pressures and Thermophysical Properties of Ethylene Carbonate, Propylene Carbonate, γ-Valerolactone, and γ-Butyrolactone. Journal of Chemical & Engineering Data, **62**(12), pp. 4174-4186.

RAMDHAREE, S., MUZENDA, E. and BELAID, M., 2013. A Review of the Equations of State and their Applicability in Phase Equilibrium Modeling,
, April 15-16, 2013 2013, International Conference on Chemical and Environmental Engineering, pp. 84-87.

RAREY, J., GMEHLING, J., KLEIBER, M. and KOLBE, B., 2012. Chemical Thermodynamics for Process Simulation: For Process Simulation. Wiley-VCH Verlag GmbH.

RIDDICK, J.A. and BUNGER, W.B., 1970. Organic Solvents: Physical Properties and Methods of Purification, 3rd edition. Wiley Interscience, New York.

SALEHPOUR, S. and DUBÉ, M.A., 2008. Biodiesel: a green polymerization solvent. Green Chemistry, **10**(3), pp. 321-326.

SAPAKALE, G.N., PATIL, S.M., SURWASE, U.S. and BHATBHAGE, P.K., 2010. A REVIEW SUPERCRITICAL FLUID EXTRACTION. Int. J. Chem. Sci, **8**(2), pp. 729-743.

SJOSTROM, E., 2013. Wood chemistry: fundamentals and applications. Elsevier.

SMITH, J.M., NESS, H.V., ABBOTT, M. and SWIHART, M., eds, 2018. Introduction to Chemical Engineering Thermodynamics. 8th edn. New York, NY: McGraw-Hill Education.

SMITH, J.M., VAN NESS, H.C. and ABBOTT, M.M., 2005. Introduction to chemical engineering thermodynamics. 7th edition edn. McGraw-Hill.

SMITH, R., 2005. Chemical process design and integration. 1st edn. The Atrium, Southern Gate, Chichester, West Sussex PO19 8SQ, England: John Wiley & Sons Ltd.

SONNENBERG, A., BAARS, J. and HENDRICKX, P., 2007. IEA Bioenergy Task 42 Biorefinery. Avantium, Biomass Research and Wageningen University and Research Centre, Netherlands, pp. 1-24.

STAHL, E., SCHUETZ, E. and MANGOLD, H.K., 1980. Extraction of seed oils with liquid and supercritical carbon dioxide. Journal of Agricultural and Food Chemistry, **28**(6), pp. 1153-1157.

STÖCKER, M., 2008. Biofuels and biomass-to-liquid fuels in the biorefinery: Catalytic conversion of lignocellulosic biomass using porous materials. Angewandte Chemie International Edition, **47**(48), pp. 9200-9211.

TANG, X., ZENG, X., LI, Z., HU, L., SUN, Y., LIU, S., LEI, T. and LIN, L., 2014. Production of γ-valerolactone from lignocellulosic biomass for sustainable fuels and chemicals supply.

TEJA, A. and J HOLM, L., 2018. Vapour-Liquid Equilibrium: Theory. 2000 Academic Press.

THE NEED PROJECT, 2017. Biomass, Secondary Energy Infobook. 8408 Kao Circle, Manassas, VA 20110: www.NEED.org.

THORE, B., SANDÉN, B., OLSSON, L. and ÅSBLAD, A., 2012. What is a biorefinery? .

WEIDLICH, U. and GMEHLING, J., 1987. A modified UNIFAC model. 1. Prediction of VLE, hE, and .gamma..infin. Industrial & Engineering Chemistry Research, **26**(7), pp. 1372-1381.

WITKOWSKI, A., 2015. Advances in carbon dioxide compression and pipeline transportation processes. Springer.

Appendix 1

Table 22: Temperature independent properties of main components Carbon dioxide, GVL, Furfural and water ((Design Institute for Physical Properties, Sponsored,by AIChE c)

		Components			
		Carbon-dioxide	**GVL**	**Fufural**	**Water**
Physical Constants	**Units**	**Values**	**Values**	**Values**	**Values**
Melting Point	K	216.60	242.15	236.65	273.15
Liquid Molar Volume @ 298 K	m^3/kmol	0.06	0.10	0.08	0.02
Boiling Point, Normal	K	194.70	480.65	434.85	373.15
Solubility Parameter @ 298 K	$(J/m^3)1/2$	14560.00	23010.00	23530.00	47860.00
Thermodynamic Properties					
The entropy of Ideal Gas @ 298 K	J/(kmol K)	2.14E+05	3.50E+05	3.33E+05	1.89E+05
Absolute Entropy of Ideal Gas @ 298 K	J/(kmol K)	2.14E+05	2.37E+05	2.18E+05	6.99E+04
Gibbs Energy of Formation of Ideal Gas @ 298 K	J/kmol	-3.90E+08	-3.00E+08	-1.00E+08	-2.29E+08
Standard Gibbs Energy of Formation @ 298 K	J/kmol	-3.90E+08	-3.10E+08	-1.20E+08	-2.37E+08
Standard Enthalpy of Formation @ 298 K	J/kmol	-3.90E+08	-4.60E+08	-2.00E+08	-2.86E+08
Enthalpy of Formation of Ideal Gas @ 298 K	J/kmol	-3.90E+08	-4.20E+08	-1.50E+08	-2.42E+08
Enthalpy of Fusion @ Melting Point	J/kmol	9.02E+05	-2.50E+09	1.44E+07	6.00E+06
Enthalpy of Sublimation	J/kmol	2.40E+07	5.57E+07	6.12E+07	5.08E+07
Triple Point Temperature	K	216.58	242.15	236.65	273.16
Triple Point Pressure	Pa	5.18E+05	0.31	1.55	611.73
Critical Properties and Acentric Factor					
Critical Temperature	K	304.21	727.00	670.15	647.10
Critical Pressure	MPa	7.38	4.84	5.66	22.06
Critical Volume	m3/kmol	0.09	0.28	0.25	0.06
Critical Compressibility		0.27	0.22	0.26	0.23
Acentric Factor ω	K	0.22	0.40	0.37	0.34

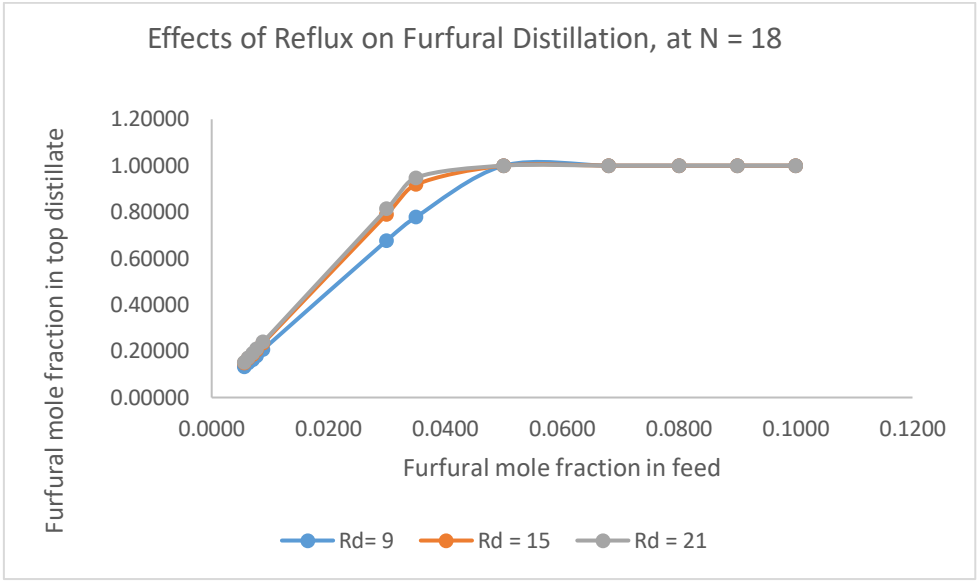

Figure 37 Effect of reflux ratio on furfural mole fraction at N = 18

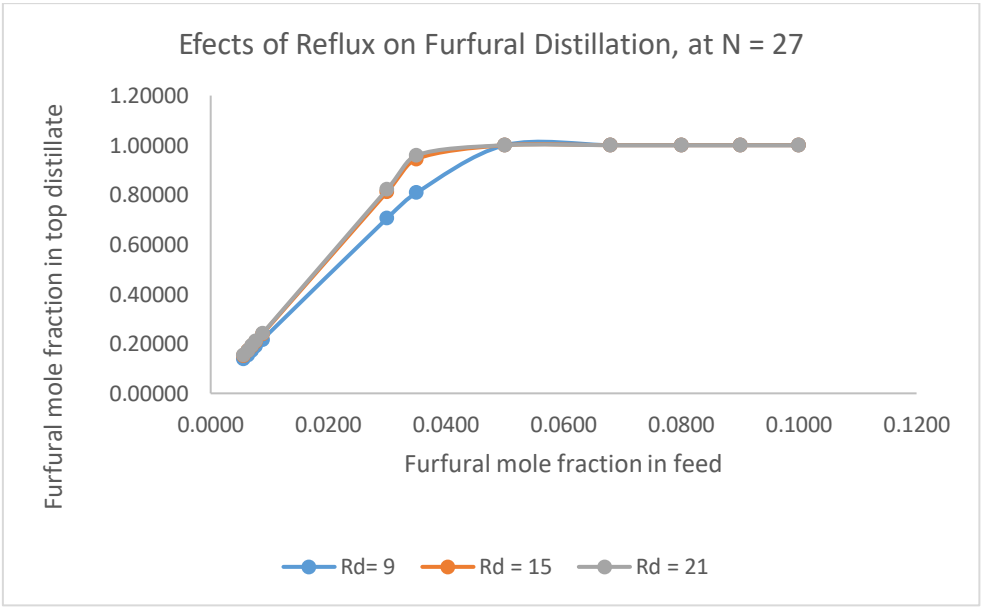

Figure 38 Effect of reflux ratio on furfural mole fraction at N = 27

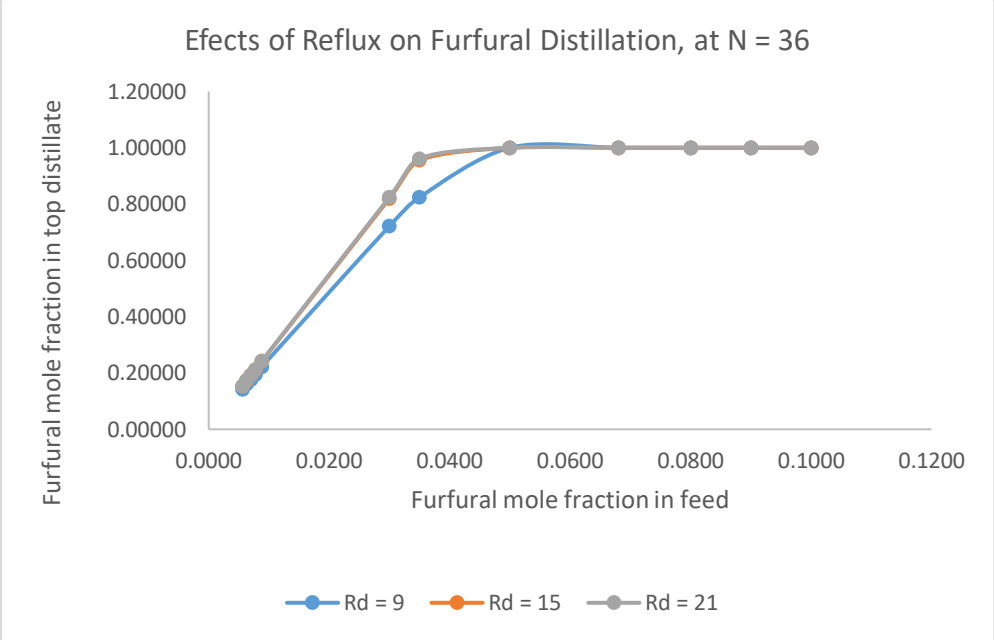

Figure 39 Effect of reflux ration on Furfural mole fraction at N = 36

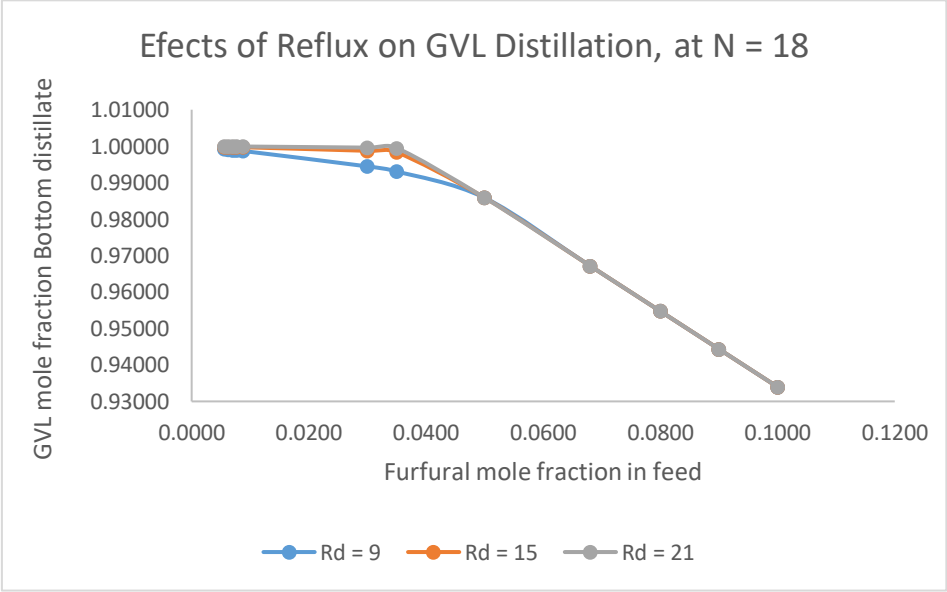

Figure 40 Effect of reflux ration on GVL mole fraction at bottom distillate at N =18

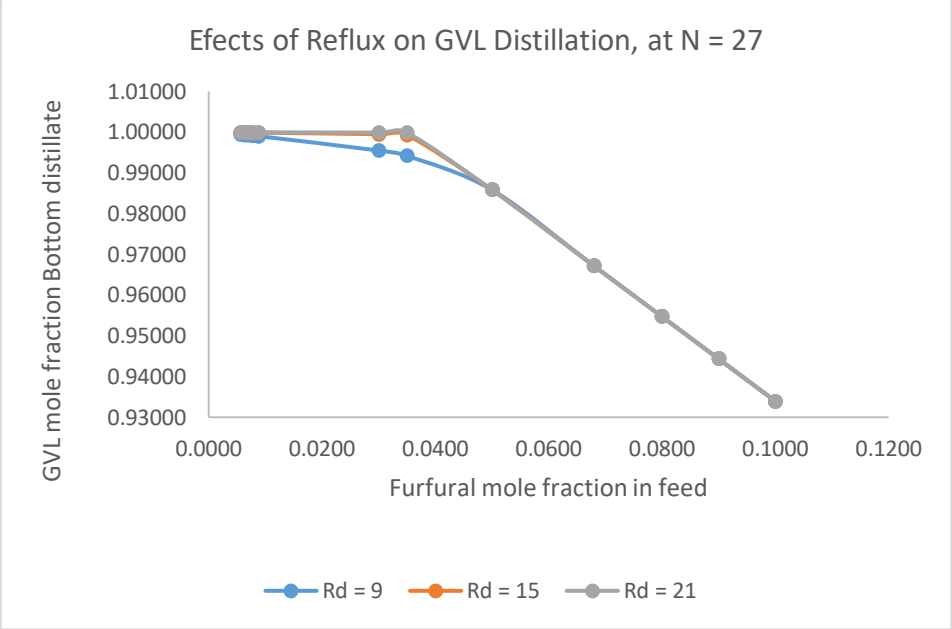

Figure 41 Effect of reflux ration on GVL mole fraction at bottom distillate at N = 27

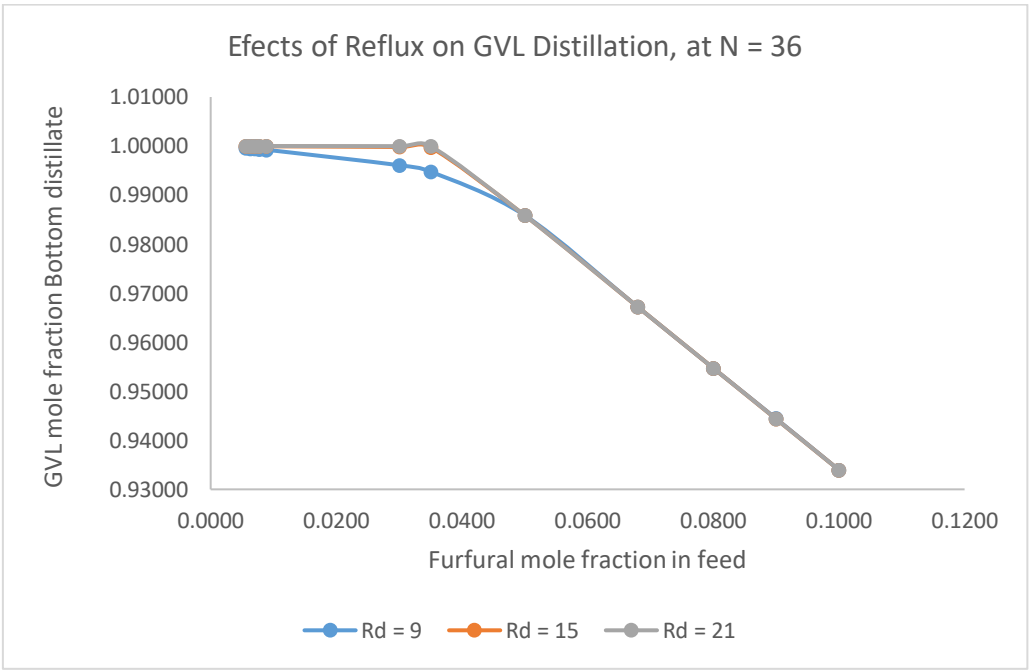

Figure 42 Effect of reflux ratio on GVL mole fraction at bottom distillate at N = 36

Appendix 2

Table 23: the effect of feed composition on the purity of GVL and furfural recovery

Serial No.	Inlet		Outlet				Q_C	Q_R
	Feed mole fraction		Top Mole fraction		Bottom mole fraction			
	Furfural	**GVL**	**Furfural, Top**	**GVL, Top**	**Furfural, Bottom**	**GVL, Bottom**		
1	0.0056	0.9944	0.14391	0.85609	0.00038	0.99962	-274247.76	274474.90
2	0.0063	0.9937	0.16191	0.83809	0.00043	0.99957	-274636.03	274916.13
3	0.0070	0.9930	0.17989	0.82011	0.00048	0.99952	-274956.51	275294.29
4	0.0077	0.9923	0.19787	0.80213	0.00052	0.99948	-275218.90	275618.31
5	0.0088	0.9912	0.22610	0.77390	0.00060	0.99940	-275520.12	276023.86
6	0.0300	0.9700	0.75602	0.24398	0.00260	0.99740	-265626.42	269008.95
7	0.0350	0.9650	0.87420	0.12580	0.00333	0.99667	-260653.47	264789.42
8	0.0500	0.9500	0.99996	0.00004	0.01415	0.98585	-254378.74	259091.98
9	0.0680	0.9320	0.99998	0.00002	0.03283	0.96717	-254377.54	258679.30
10	0.0800	0.9200	0.99998	0.00002	0.04528	0.95472	-254377.32	258430.22
11	0.0900	0.9100	0.99999	0.00001	0.05566	0.94434	-254377.20	258231.45
12	0.1000	0.9000	0.99999	0.00001	0.06604	0.93396	-254377.11	258043.69

Table 24: The effect of reflux ratio on the purity of GVL and furfural recovery for N = 9

No. of plates	Inlet		Furfural mole fraction, Top			GVL mole fraction, Bottom		
	Feed composition, mole fraction		Reflux Ratio, Rd			Reflux Ratio, Rd		
	Furfural	**GVL**	**9**	**15**	**21**	**9**	**15**	**21**
9	0.0056	0.9944	0.11850	0.13804	0.14523	0.99866	0.99940	0.99967
9	0.0063	0.9937	0.13326	0.15528	0.16337	0.99849	0.99932	0.99963
9	0.0070	0.9930	0.14801	0.17250	0.18151	0.99832	0.99925	0.99958
9	0.0077	0.9923	0.16272	0.18971	0.19963	0.99815	0.99917	0.99954
9	0.0088	0.9912	0.18582	0.21671	0.22809	0.99788	0.99905	0.99948
9	0.0300	0.9700	0.60378	0.71468	0.75896	0.99165	0.99584	0.99751
9	0.0350	0.9650	0.68990	0.81485	0.86467	0.98971	0.99443	0.99631
9	0.0500	0.9500	0.88254	0.95874	0.97565	0.98142	0.98429	0.98493
9	0.0680	0.9320	0.95606	0.98130	0.98799	0.96551	0.96646	0.96672
9	0.0800	0.9200	0.96991	0.98587	0.99065	0.95358	0.95418	0.95436
9	0.0900	0.9100	0.97605	0.98811	0.99199	0.94344	0.94389	0.94404
9	0.1000	0.9000	0.98002	0.98966	0.99293	0.93321	0.93357	0.93370

Table 25: The effect of reflux ratio on the purity of GVL and furfural recovery for N = 18

No. of plates	Inlet		Furfural mole fraction, Top			GVL mole fraction, Bottom		
	Feed composition, mole fraction		Reflux Ratio, Rd			Reflux Ratio, Rd		
	Furfural	GVL	9	15	21	9	15	21
18	0.0056	0.9944	0.13181	0.14902	0.15238	0.99916	0.99981	0.99994
18	0.0063	0.9937	0.14826	0.16765	0.17144	0.99906	0.99979	0.99993
18	0.0070	0.9930	0.16470	0.18629	0.19049	0.99895	0.99977	0.99992
18	0.0077	0.9923	0.18110	0.20492	0.20954	0.99884	0.99974	0.99992
18	0.0088	0.9912	0.20684	0.23418	0.23947	0.99867	0.99970	0.99991
18	0.0300	0.9700	0.67803	0.79105	0.81426	0.99445	0.99872	0.99960
18	0.0350	0.9650	0.77874	0.91861	0.94862	0.99307	0.99834	0.99948
18	0.0500	0.9500	0.99974	0.99998	0.99999	0.98584	0.98585	0.98585
18	0.0680	0.9320	0.99995	0.99999	0.99999	0.96717	0.96717	0.96717
18	0.0800	0.9200	0.99997	0.99999	0.99999	0.95472	0.95472	0.95472
18	0.0900	0.9100	0.99997	0.99999	0.99999	0.94434	0.94434	0.94434
18	0.1000	0.9000	0.99998	0.99999	1.00000	0.93396	0.93396	0.93396

Table 26: The effect of reflux ratio on the purity of GVL and furfural recovery for N = 27

No. of plates	Inlet		Furfural mole fraction, Top			GVL mole fraction, Bottom		
	Feed composition, mole fraction		Reflux Ratio, Rd			Reflux Ratio, Rd		
	Furfural	GVL	9	15	21	9	15	21
27	0.0056	0.9944	0.13792	0.15227	0.15367	0.99939	0.99994	0.99999
27	0.0063	0.9937	0.15513	0.17131	0.17288	0.99932	0.99993	0.99999
27	0.0070	0.9930	0.17232	0.19035	0.19209	0.99924	0.99992	0.99999
27	0.0077	0.9923	0.18949	0.20938	0.21130	0.99916	0.99991	0.99998
27	0.0088	0.9912	0.21644	0.23930	0.24149	0.99904	0.99990	0.99998
27	0.0300	0.9700	0.70575	0.81195	0.82265	0.99550	0.99951	0.99991
27	0.0350	0.9650	0.80859	0.94470	0.95933	0.99419	0.99933	0.99988
27	0.0500	0.9500	1.00000	1.00000	1.00000	0.98585	0.98585	0.98585
27	0.0680	0.9320	1.00000	1.00000	1.00000	0.96717	0.96717	0.96717
27	0.0800	0.9200	1.00000	1.00000	1.00000	0.95472	0.95472	0.95472
27	0.0900	0.9100	1.00000	1.00000	1.00000	0.94434	0.94434	0.94434
27	0.1000	0.9000	1.00000	1.00000	1.00000	0.93396	0.93396	0.93396

Table 27 The effect of reflux ratio on the purity of GVL and furfural recovery for N = 36

No. of plates	Inlet		Furfural mole fraction, Top			GVL mole fraction, Bottom		
	Feed composition, mole fraction		Reflux Ratio, Rd			Reflux Ratio, Rd		
	Furfural	GVL	9	15	21	9	15	21
36	0.0056	0.9944	0.14153	0.15339	0.15393	0.99953	0.99998	1.00000
36	0.0063	0.9937	0.15919	0.17256	0.17317	0.99947	0.99997	1.00000
36	0.0070	0.9930	0.17684	0.19174	0.19242	0.99941	0.99997	1.00000
36	0.0077	0.9923	0.19445	0.21092	0.21166	0.99935	0.99997	1.00000
36	0.0088	0.9912	0.22207	0.24105	0.24190	0.99925	0.99996	1.00000
36	0.0300	0.9700	0.72150	0.81997	0.82449	0.99609	0.99981	0.99998
36	0.0350	0.9650	0.82423	0.95528	0.96178	0.99478	0.99973	0.99997
36	0.0500	0.9500	1.00000	1.00000	1.00000	0.98585	0.98585	0.98585
36	0.0680	0.9320	1.00000	1.00000	1.00000	0.96717	0.96717	0.96717
36	0.0800	0.9200	1.00000	1.00000	1.00000	0.95472	0.95472	0.95472
36	0.0900	0.9100	1.00000	1.00000	1.00000	0.94443	0.94434	0.94434
36	0.1000	0.9000	1.00000	1.00000	1.00000	0.93396	0.93396	0.93396

Appendix 3:

Table 28: Result summary of the liquid-liquid extraction using liquid CO_2

	Units	AQS1	AQS2	CO2SOLV	EXTR	FEED	ORGS2	ORGS3	REFF
From		STAGE1	STAGE2		STAGE1		STAGE2	STAGE3	STAGE3
To		STAGE2	STAGE3	STAGE3		STAGE1	STAGE1	STAGE2	
Phase:		Liquid	Liquid	Liquid	Liquid	Liquid	Liquid	Liquid	Liquid
Component Mole Flow									
CARBO-01	kmol/sec	0.0077	0.0071	0.1657	0.1595	0	0.1672	0.1666	0.0062
GAMMA-01	kmol/sec	0.0016	0.0002	0	0.013	0.0131	0.0015	0.0001	0.0001
WATER	kmol/sec	0.2236	0.2222	0	0.0058	0.2271	0.0023	0.0009	0.2213
Mole Flow	kmol/hr	838	826	597	642	864	616	604	819
Mass Flow	kg/hr	16324	15686	26260	29941	19123	27142	26504	15442
Volume Flow	CUM/sec	0.0045	0.0043	0.0101	0.0086	0.0054	0.0093	0.0099	0.0042
Temperature	K	298.15	298.15	298.15	298.15	298.15	298.15	298.15	298.15
Pressure	MPa	7.5	7.5	7.5	7.5	7.5	7.5	7.5	7.5
Vapour Fraction		0	0	0	0	0	0	0	0
Liquid Fraction		1	1	1	1	1	1	1	1
Solid Fraction		0	0	0	0	0	0	0	0
Molar Enthalpy	kJ/mol	-291	-290	-404	-405	-296	-403	-403	-289
Mass Enthalpy	kJ/kg	-14973	-15317	-9173	-8569	-13152	-9124	-9178	-15406
Enthalpy Flow	kW	-67714	-66438	-66908	-72185	-70997	-68861	-67580	-65767
Molar Entropy	kJ/kmol-K	-161	-160	-63	-97	-182	-67	-64	-160
Mass Entropy	kJ/kg-K	-8.3	-8.44	-1.43	-2.06	-8.11	-1.53	-1.45	-8.52
Molar Density	kmolL/CUM	52	53	16	21	45	18	17	54
Mass Density	kg/CUM	1010	1009	721	977	1007	807	740	1007
Average Molecular Weight		19.42	18.9	44.01	47.24	22.48	44.14	43.92	18.76